Acta Pharmaceutica Sinica B 2023;13(7):3008−3026

Chinese Pharmaceutical Association
Institute of Materia Medica, Chinese Academy of Medical Sciences

Acta Pharmaceutica Sinica B

www.elsevier.com/locate/apsb
www.sciencedirect.com

ORIGINAL ARTICLE

Glutamate-releasing BEST1 channel is a new target for neuroprotection against ischemic stroke with wide time window

Shuai Xiong[a,†], Hui Xiao[a,†], Meng Sun[a], Yunjie Liu[a], Ling Gao[a], Ke Xu[a], Haiying Liang[a], Nan Jiang[b], Yuhui Lin[a], Lei Chang[a], Haiyin Wu[a,c], Dongya Zhu[a,c], Chunxia Luo[a,c,*]

[a]*Department of Pharmacology, School of Pharmacy, Nanjing Medical University, Nanjing 211166, China*
[b]*Department of Medicinal Chemistry, School of Pharmacy, Nanjing Medical University, Nanjing 211166, China*
[c]*Collaborative Innovation Center for Cardiovascular Disease Translational Medicine, Nanjing Medical University, Nanjing 211166, China*

Received 18 October 2022; received in revised form 13 January 2023; accepted 3 April 2023

KEY WORDS

BEST1;
Ischemic stroke;
Glutamate release;
Delayed excitotoxicity;
Infarct expansion;
Neurological functions;
Calcium-activated chloride channels

Abstract Many efforts have been made to understand excitotoxicity and develop neuroprotectants for the therapy of ischemic stroke. The narrow treatment time window is still to be solved. Given that the ischemic core expanded over days, treatment with an extended time window is anticipated. Bestrophin 1 (BEST1) belongs to a bestrophin family of calcium-activated chloride channels. We revealed an increase in neuronal BEST1 expression and function within the peri-infarct from 8 to 48 h after ischemic stroke in mice. Interfering the protein expression or inhibiting the channel function of BEST1 by genetic manipulation displayed neuroprotective effects and improved motor functional deficits. Using electrophysiological recordings, we demonstrated that extrasynaptic glutamate release through BEST1 channel resulted in delayed excitotoxicity. Finally, we confirmed the therapeutic efficacy of pharmacological inhibition of BEST1 during 6−72 h post-ischemia in rodents. This delayed treatment prevented the expansion of infarct volume and the exacerbation of neurological functions. Our study identifies the glutamate-releasing BEST1 channel as a potential therapeutic target against ischemic stroke with a wide time window.

*Corresponding author.
E-mail address: chunxialuo@njmu.edu.cn (Chunxia Luo).
[†]These authors made equal contributions to this work.
Peer review under the responsibility of Chinese Pharmaceutical Association and Institute of Materia Medica, Chinese Academy of Medical Sciences.

https://doi.org/10.1016/j.apsb.2023.05.012

1. Introduction

Ischemic stroke is a leading cause of death and adult disability worldwide. Although the robust benefits of intravenous thrombolysis and mechanical thrombectomy for restoration of cerebral flow are demonstrated, the therapeutic options especially the potential pharmaceutical treatments for neuroprotection against acute ischemic damage remain limited[1,2]. Within the ischemic brain tissue, complex cascades resulting in irreversible damage over hours to days have been identified, involving excitotoxicity, calcium overload, oxidative stress, apoptosis, and inflammation[3−5]. For decades, many efforts have been made to the development of neuroprotective drugs for acute ischemic stroke based on the above multiple mechanisms, but few feasible treatment candidates have passed the rigorous clinical trials[6−8]. Mounting evidence has indicated that excitotoxicity mediated by glutamate accumulation in the extracellular space is a predominant factor causing the early stages of ischemic cell death, and it also contributes to calcium influx and superoxide anion generation after *N*-methyl-D-aspartate receptor (NMDARs) activation[3,9]. We have demonstrated that uncoupling the downstream signaling cascade of NMDARs is effective against animal stroke damage[10], and the ESCAPE-NA1 trial on efficacy and safety of nerinetide, an eicosapeptide designed to perturb the protein−protein interactions of NMDARs and post-synaptic density protein 95 (PSD-95), for the treatment of human acute ischemic stroke further validate the possibility of clinical translation for excitotoxicity hypothesis[11,12].

Apart from glutamate receptors, glutamate release is more upstream initiation point for excitotoxicity during ischemic stroke. However, the direct inhibition of synaptic glutamate release with magnesium ions[13], N-type calcium channel antagonist ziconotide[14] and sodium channel blocker sipatrigine[15], have all failed in the clinical testing required for broad clinical use. Understanding the specific and precise extrasynaptic mechanisms underlying ischemia-induced glutamate release will allow the improvement of potential therapeutic opportunities and treatment targets. It is well known that reversed operation of glutamate transporters in severe brain ischemia mainly account for the elevation of extrasynaptic glutamate levels from glial or neuronal origins a few minutes after the start of ischemia[16−18]. In addition to their role in ischemic glutamate release, these glutamate transporters are also essential for glutamate uptake and clearance during normal synaptic transmission and even under ischemia[9,19]. Thus, chronic inhibition of the glutamate uptake system by pharmaceutical or genetic treatment induces excitotoxicity and exacerbates ischemic neuronal death[20−22], while increased expression or activity of glutamate transporter-1 (GLT-1) protects neurons against ischemic injury[23,24]. Selective prevention of reversed operation of glutamate transporters is suggested as a new strategy for the therapy of ischemic stroke[19]. Besides, the researches on other mechanisms mediating ischemic glutamate release have made progress. Recently, extrasynaptic glutamate release through cystine/glutamate antiporter[25] and volume-regulated anion channel SWELL1[26] is reported to promote ischemic damage. These glutamate-releasing approaches are almost stimulated within several minutes to hours, leading to narrow time window for neuroprotective treatment, though they are critical to the irreversible injury ultimately resulting in the infarction. We found that the extracellular glutamate level is still elevated until 8 days after photothrombotic stroke[27], indicating a delayed glutamate release mechanism should exist after the immediate events. No attention is paid to the implication of such glutamate release in the exacerbation of ischemic damage. By RNA sequencing of peri-infarct cortex extracts from ischemic animals, we screened out a candidate bestrophin 1 (BEST1)[27].

BEST1 belongs to a bestrophin family of calcium-activated chloride channels (CaCCs), first identified in the retina with an implication in human vitelliform macular dystrophy[28−30]. Subsequently, most of the studies on the bestrophins have been concentrated on its expression and function in the eye. In human, brain is the organ where the mRNA and protein abundance of BEST1 is second only to the retina[31]. Until recently, evidence suggests the role of BEST1 in the brain. Mouse *Best1* mRNA was widely distributed in the brain, especially with higher levels in olfactory bulb, hippocampus, and cerebellum and prominent expression in both neurons and astrocytes[32]. In the brain, the most prominent feature of BEST1 is its significant permeability to glutamate and γ-amino butyric acid (GABA) in addition to Cl^-[33−35]. Under pathological conditions, such as Alzheimer's disease[36], epileptic seizures[37] and subcortical ischemic stroke[38], BEST1-mediated tonic GABA release from astrocytes is demonstrated to be important to the modulation of neuronal excitability and synaptic plasticity. Particularly, excessive GABA through astrocytic BEST1 impedes functional recovery after stroke[38]. Moreover, BEST1 in dorsal root ganglia neurons was reported to be a positive player in the regenerative process of the mechanosensitive afferent fibers after peripheral nerve axotomy[39,40]. However, the contribution of BEST1-mediated glutamate release to acute ischemic damage has not been elucidated.

Here, we discovered a neuron-specific increase of BEST1 expression within the peri-infarct from 8 to 48 h after ischemic stroke in mice and explored its role in ischemic neuronal damage and motor functional deficits with shRNA interference. Moreover, we investigated the relationship between the glutamate release and the Cl^- permeability of BEST1 channel and illustrated the contribution of extrasynaptic glutamate release through BEST1 to the exacerbation of ischemic damages by enhancement of tonic excitation. Finally, we evaluated the therapeutic efficacy of pharmacological inhibition of BEST1 during 6−72 h post-ischemia in mice and rats. This study indicates that glutamate-releasing BEST1 channel is a new target for neuroprotection against ischemic damage with a wide time window.

2. Materials and methods

2.1. Animals

Male C57BL/6 mice (Model Animal Research Center of Nanjing University, Nanjing, China) were used for PT models, 6- to

7-weeks old in AAVs-infected experiments and 8- to 9-weeks old in other experiments. Male Sprague−Dawley rats (9- to 10-week old, Slac Laboratory Animal, Shanghai, China) were used for MCAO models. Embryonic C57BL/6 mice (E16, both male and female) were used for neuron cultures. Animals were maintained at a controlled temperature (20 ± 2 °C) and group-housed them (12-h light-dark cycle) with access to food and water *ad libitum*. Every effort was made to minimize the number of animals used and their suffering. All animal experiments were approved by the Institutional Animal Care and Use Committee of Nanjing Medical University (No. IACUC-2111020).

2.2. Drugs and reagents

5-Nitro-2-(3-phenylpropylamino) benzoic acid (NPPB, Sigma−Aldrich, St. Louis, MO, USA; Cat# N4779) and 4,4′-diisothio-cyanostilbene-2,2′-disulfonic acid (DIDS, Sigma−Aldrich; Cat# D3514) were used to block Cl^- channels in electrophysiological recordings (NPPB, dissolved in DMSO and the diluted with ACSF to 100 μmol/L) and animal experiments (DIDS, 12 mg/kg, dissolved in DMSO and then diluted in PBS with 10% polysorbate 80). All other drugs and reagents used in electrophysiological recordings, Western blot assay, and immunofluorescence were purchased from Sigma−Aldrich or Tocris Bioscience (Avonmouth, Bristol, UK).

2.3. Focal ischemia models

Focal ischemia was induced by photothrombosis (PT) of cortical microvessels in mice and by middle cerebral artery occlusion (MCAO) in rats or mice, as we described previously.

2.3.1. Photothrombotic ischemia (PT)

Focal cortical ischemia was performed as we described previously[27,41]. Mice were kept anesthetized with 1.5% isoflurane, and placed in a stereotaxic device (Stoelting, Kiel, WI, USA). The skull was exposed by incising the midline, clearing connective tissue and keeping the surface dry. A cold light source (World Precision Instruments, Sarasota, FL, USA) attached to an opaque template with an opening for giving a 2-mm diameter illumination was positioned −1.5 mm lateral from Bregma. Five minutes after Rose Bengal solution (Sigma−Aldrich; 100 mg/kg, i.p.) was administered, the brain was illuminated through the intact skull. The illuminance was 10,000 lux × 12 min for AAVs-infected experiments and 12,000 lux × 15 min for others. Through light excitation, singlet oxygen was generated from Rose Bengal, which damages and occludes vascular endothelium, leading to focal cortical ischemia. Control mice received the same dose of Rose Bengal without illumination.

2.3.2. Middle cerebral artery occlusion (MCAO)

To induce ischemia−reperfusion stroke, intraluminal MCAO was performed[10,27]. Briefly, rats were kept anesthetized with 2% isoflurane and a 4/0 (for rats) or 8/0 (for mice) surgical nylon monofilament with a rounded tip was introduced into the left internal carotid artery through the external carotid stump, advanced 20−21 mm (in rats) or 10−11 mm (in mice) past the carotid bifurcation until a slight resistance was felt. The filament was left in place for 120 min (for rats) or 60 min (for mice) and then withdrawn for reperfusion. Regional cerebral blood flow was monitored by a laser Doppler perfusion monitor (Moor Instruments, Wilmington, DE, USA) to ensure that the regional cerebral blood flow decreased by 85%−95%. Sham-operated rats received the same procedure as MCAO rats except that the occluding filament was inserted only 7 mm above the carotid bifurcation.

2.4. Recombinant virus and stereotaxic injection

Short hairpin RNAs targeting mouse *Best1* were synthesized as follows: 5′-tttgccaacttgtcaatgaattcaagagatcattgacaagttggcaatttttc-3′ and 5′-tcgagaaaaaatcgcatagcgtatgccgtttctcttgaaaacggcatacgctatg cgaa-3′[32,33]. Recombinant AAV-CMV-sh*Best1*-GFP was generated by GeneChem Co., Ltd. (Shanghai, China) to knockdown BEST1 expression *in vivo*. Moreover, recombinant AAV-Flex-sh*Best1*-GFP (Obio Technology, Shanghai, China) was generated for specific knockdown of BEST1 expression in neurons *in vivo*, combined with AAV-Syn-Cre (GeneChem). AAV-CMV-BEST1^{WT}-3Flag-T2A-GFP expressing 3Flag-tagged wild type mouse BEST1 and AAV-CMV-BEST1^{W93C}-3Flag-T2A-GFP expressing 3Flag-tagged mouse BEST1 with a point mutation (tryptophan-93 to cysteine-93) were products of GeneChem. The BEST1^{W93C} mutation has been proven to impair the CaCC currents for BEST1[32,33,42]. Fourteen days before PT ischemia induction to mice, desired AAV (1×10^{13} v.g./mL, 1 μL) was delivered into cortex (anterior-posterior, 0 mm; medial-lateral, −1.5 mm; dorsal-ventral, 1.5 mm) using a stereotaxic instrument (Stoelting, Wood Dale, IL, USA) at a rate of 2 nL/s to produce an infection of peri-infarct region. The needle was withdrawn over a course of 10 min to assure even distribution of the virus. For mice MCAO experiment, AAV (1×10^{13} v.g./mL, 1 μL/site) was microinjected into 3 sites to obtain a wide infection (anterior-posterior, 1.5, 0.3, −0.9 mm; medial-lateral, −2.5, −2.5, −2.5 mm; dorsal-ventral, 2.5, 2.2, 2.0 mm). Whether the desired brain region was correctly targeted was confirmed by immunofluorescence of GFP using 5 mice in a preliminary experiment. In the formal experiments, only the suspected mice with abnormal behavioral data were examined. If the peri-infarct zone was not correctly targeted, the mouse was excluded from statistical analysis.

2.5. Behavioral assessments

The motor function of mice was assessed by grid-walking task and cylinder task[27,41] one day before PT operation (for baseline) and 3 days after ischemia (for functional deficits). Two days after MCAO, animal neurological deficits were scored[8]. All assessments were performed in a blinded manner.

2.5.1. Grid-walking task

A 12-mm square wire mesh with a grid area (length, 32 cm; width, 20 cm; height, 50 cm) was manufactured as the apparatus to conduct the grid-walking task. A camera was positioned beneath the device to video footage in order to assess the stepping errors (foot faults). Each mouse was placed individually on the top of the elevated wire grid and allowed to freely move until at least 100 steps have been taken by the left forelimb. If a step was not providing support and the foot went through the grid hole, this was considered a fault. A step was also considered a foot fault if an animal was resting with the grid at the level of the wrist. Analysis was performed offline by a rater blind to group design. The number of foot-fault steps and the number of total steps (foot-fault steps and non-foot-fault steps) for the left forelimb and right

forelimb were counted and the ratio between foot-fault steps and total steps was calculated.

2.5.2. Cylinder task

Each mouse was placed individually in a clear plexiglass cylinder (height, 15 cm; diameter, 10 cm) and the spontaneous use of either one or both forelimbs for vertical wall exploration was encouraged in the cylinder task. Each mouse was allowed to freely explore until at least 20 s of rears in the cylinder and videotaped. The video was analyzed offline by calculating the time (s) during each rear that each animal spent on either the right forelimb, the left forelimb, or both forelimbs in slow motion (1/5th real-time speed). Only rears in which both forelimbs could be clearly seen were included in our analysis. The time spent on each forelimb and both forelimbs were calculated, and these data were used to derive an asymmetry index: (time spent on right forelimb − time spent on left forelimb)/total time spent on either one or both forelimbs.

2.5.3. Neuroscore assessment

Neurological deficits of animals after MCAO were scored by an experimenter blinded to the experimental groups as we previous did[10]. Rating scale: 0 = no deficit, 1 = failure to extent left forepaw, 2 = decreased grip strength of left forepaw, 3 = circling to left by pulling the tail, and 4 = spontaneous circling.

2.6. Western blot

Western bolt analysis was performed as before[43]. Tissues from peri-infarct cortex were lysed in 100 mmol/L HEPES containing 200 mmol/L NaCl, 10% glycerol, 2 mmol/L $Na_4P_2O_7$, 2 mmol/L DTT, 1 mmol/L EDTA, 1 mmol/L benzamidine, 0.1 mmol/L Na_3VO_4, 1 μmol/L pepstatin, 10 μg/mL aprotinin, 10 μg/mL leupeptin and 10 μmol/L PMSF at PH 7.4. After lysis for 30 min in ice, samples were centrifuged at 12,000 × *g*, 4 °C for 15 min. The samples containing equivalent amounts of protein were applied to acrylamide denaturing gels (SDS-PAGE). The separated proteins were transferred onto Immobilon-P Transfer Membranes (Millipore, Burlington, MA, USA). Blotting membranes were incubated with blocking solution [7.5% nonfat dried milk powder dissolved in PBST buffer (pH 7.5, 10 mmol/L Tris-HCl, 150 mmol/L NaCl, and 0.1% Tween 20)] for 1 h at room temperature, washed three times, and then were incubated with primary antibodies in PBST overnight at 4 °C. After several washes with PBST buffer, the membranes were incubated for 2 h with appropriate horseradish peroxidase-linked secondary antibody. The membranes were then processed with enhanced chemiluminescence western blotting detection reagents (Bio-Rad, Hercules, CA, USA). The films were scanned with ChemiDOC MP Imaging System (Bio-Rad), avoiding densitometric saturation, and densitometry was performed using Image Lab software (Bio-Rad). Primary antibodies used were rabbit anti-BEST1 (1:1000; Cohesion, Cat# CPA9240), rabbit anti-β-actin (1:2000; Bioss, Cat# bs-0061R, RRID: AB_10855480), rabbit anti-GLT-1 (1:1000, Abcam, Cat# ab41621, RRID: AB_941782); rabbit anti-GluN2B (1:4000, Cell Signaling Technology, Cat# 4207, RRID: AB_1264223); and mouse anti-GAPDH (1:8000, Kangcheng, Cat# KC-5G4, RRID: AB_2493106). Secondary antibody used was goat anti-rabbit HRP (1:15,000; Multi Science, Cat# GAR0072) and goat anti-mouse HRP (1:15,000, Multi Science, Cat# GAM0072, RRID: AB_2827834).

2.7. Immunofluorescence, cell counting and morphological analysis

Immunofluorescence labeling for brain sections and cultured cells was performed as we previously did[41,43].

Mice were transcardially perfused with 4% paraformaldehyde (*w/v*) in phosphate buffer (0.1 mol/L, pH 7.4), and brains were removed and post-fixed overnight. Serial vibratome sections (40 μm) were processed. After blocking in PBS containing 3% normal goat serum, 0.3% (*w/v*) Triton X-100 and 0.1% BSA at room temperature for 1 h, slices were incubated in primary antibody diluted in blocking solution overnight at 4 °C and washed. Slices were then incubated in secondary antibody for 2 h at room temperature. Finally, slices were mounted onto slides and images were acquired with a fluorescence microscope (Axio Imager, Zeiss, Oberkochen, Germany) or a confocal laser-scanning microscope (LSM700, Zeiss). For $NeuN^+$ cells counting within peri-infarct cortex, 3 directions (4 o'clock, 6 o'clock and 8 o'clock) were selected to capture images in one slice and 3 typical slices (front, middle and rear) were chosen to represent an animal. The images were analyzed with Image-Pro Plus software (Media Cybernetics, Silver Spring, MD, USA) by an experimenter blind to the treatment of groups.

Fixed cultures were blocked in PBS containing 3% normal goat serum, 0.3% (*w/v*) Triton X-100 and 0.1% BSA at room temperature for 1 h, and incubated with primary antibody at 4 °C overnight. Subsequently, cells were incubated with secondary antibodies for 2 h at room temperature. Finally, cells were imaged with a fluorescence microscope (Axio Imager, Zeiss) or a confocal laser-scanning microscope (LSM700, Zeiss) and analyzed with Imaris 7.3.0 software (Bitplane Scientific Software) by an experimenter blind to the treatment of groups. The morphological data of spine density and $synapsin^+$/$PSD\text{-}95^+$ puncta density were obtained from 3 independently cultured samples (9−10 cells systematically across the dish for each sample were included in statistics).

Primary antibodies used were as follows: rabbit anti-BEST1 (1:100, Abcam, Cat# ab14927, RRID: AB_301518), rabbit anti-BEST1 (1:200; Cohesion, Cat# CPA9240), chicken anti-GFP (1:1000; Millipore, Cat# AB16901, RRID: AB_90890), mouse anti-NeuN (1:500; millipore, Cat# MAB377, RRID: AB_2298772), chicken anti-GFAP (1:1000; Millipore, Cat# AB5541, RRID: AB_177521), rabbit anti-synapsin I (1:400; Millipore, Cat# AB1543P, RRID: AB_90757), mouse anti-PSD-95 (1:200; Abcam, Cat# ab2723, RRID: AB_303248) and mouse anti-Flag (1:400; Sigma−Aldrich, Cat# F1804, RRID: AB_262044). Secondary antibodies used were goat anti-rabbit Cy3 (1:400; Jackson ImmunoResearch, Cat# 111-165-003, RRID: AB_2338000), goat anti-mouse Cy3 (1:400; Jackson ImmunoResearch, Cat# 115-165-003, RRID: AB_2338680), goat anti-mouse Alex 647 (1:400; Jackson ImmunoResearch, Cat# 115-605-003, RRID:AB_2338902), anti-mouse DyLight 405 (1:400; Jackson ImmunoResearch, Cat# 115-475-062, RRID: AB_2338791), goat anti-chicken Alex 488 (1:400; Jackson ImmunoResearch, Cat# 103-545-155, RRID: AB_2337390), goat anti-chicken Alex 647 (1:400; Jackson ImmunoResearch, Cat# 103-605-155, RRID: AB_2337392).

2.8. Infarct volume measurements

Infarct volume was measured by NeuN staining 3 days after PT ischemia, by *in vivo* magnetic resonance imaging (MRI) 6 and

73 h after PT ischemia, or by TTC staining 2 days after MCAO ischemia. Details are described in Supporting Information.

2.8.1. NeuN staining

Following behavioral tests on Day 3 after PT ischemia, mice were sacrificed for immunofluorescence labeling with NeuN antibody. Coronal slices (40 μm) were cut using a vibrating blade microtome (VT1200s, Leica). Every 4th section throughout the infarct area was collected for NeuN staining. Images were captured with a microscope (Axio Imager, Zeiss), and infarct volume (mm^3) was calculated as: total infarct area (mm^2) × 0.16 mm.

2.8.2. Magnetic resonance imaging (MRI)

In vivo MRI was performed 6 and 73 h after PT ischemia using a small animal MRI scanner (Bruker BioSpin, Rheinstetten, Germany) as we previously described[44]. Briefly, mice were anesthetized with 1.5% isoflurane. T2-TurboRARE imaging was conducted 6 and 73 h after PT stroke using a 2D fast-spin-echo sequence (repetition time/echo time: 3000 ms/38 ms). Seventeen consecutive coronal slices with a slice thickness of 0.8 mm, a matrix size of 256 × 256, and a field of view of 22 mm × 20 mm were positioned over the brain. Infarct volume (mm^3) was calculated as: total infarct area (mm^2) × 0.8 mm. Infarct enlargement (%) from 6 to 73 h after PT surgery was calculated according to Eq. (1):

$$\text{Infarct enlargement (\%)} = (\text{Infarct volume at 73 h} - \text{Infarct volume at 6 h})/\text{Infarct volume at 6 h} \times 100 \quad (1)$$

2.8.3. TTC staining

TTC staining was carried out 2 days after MCAO ischemia as previously described[10]. In brief, brains were removed rapidly and frozen at −20 °C for 5 min. Coronal slices were made at 1−2 mm from the frontal tips, and sections were immersed in 2% TTC at 37 °C for 20 min. Infarct volume was expressed as a percentage area of the coronal section in the infracted hemisphere.

2.9. Cell cultures

All cultures were maintained in an incubator (HERAcell 150, Thermo Fisher Scientific) with humidified atmosphere of 95% air and 5% CO_2 at 37 °C, except OGD experiments.

2.9.1. Primary neurons and lentivirus infection

Primary cortex neurons were isolated and cultured as we previously described[45]. Briefly, embryonic day 16 (E16) mouse cortex was freshly isolated and enzymatically dissociated in CMF-HBSS containing 0.125% trypsin at 37 °C for 10 min. Then the digestion was terminated with DMEM/F12 (1:1) containing 10% FBS and tissues were triturated with a fire-polished glass pipet. Dissociated cells were centrifuged, resuspended in neurobasal medium (Gibco) containing 2% B27 supplement, 0.5 mmol/L L-glutamine, 5 IU penicillin, and 5 μg/mL streptomycin, and plated on 10 μg/mL polyornithine-coated dishes (diameter 3.5 cm) at 1×10^4 cells/cm^2 for morphological analysis or 1×10^5 cells/cm^2 for biochemical detection. Cultured neurons were infected with LV-CMV-shBEST1-GFP or LV-CMV-GFP containing 1.0×10^9 TU/mL on Day 4 *in vitro* (MOI = 2.5) and the Neurobasal/B27 medium was half changed 8 h later and fully changed 24 h later. During the culture stage without virus infection, half of the medium was replaced with fresh Neurobasal/B27 medium every 3−4 days.

2.9.2. HEK293 cells and plasmids transfection

HEK293 cells (FuHeng Biology, Shanghai, China, Cat# FH0242, RRID: CVCL_0045) were cultured in MEM medium supplemented with 10% FBS (Gibico), 1% L-glutamine (Gibco) and 1% mycillin (Gibco) as before[46]. For transfection, the cells were subcultured onto a 3.5 cm dish at the ratio of 1:2. Then, the plasmid pCMV-BEST1^{WT}-3Flag-T2A-GFP or pCMV-BEST1^{W93C}-3Flag-T2A-GFP (Genechem) (1 μg per mL medium) were transfected using Fugene HD transfection reagent (Promega). Cells were replated onto glass coverslips 12−18 h after transfection and used for patch-clamp recordings within 22−30 h.

2.9.3. Glia cultures

Primary glia were isolated from the cortex of neonatal mice (1-day-old) and cultured as we reported previously[41]. Briefly, neonatal mice were decapitated and their brains were quickly removed and enzymatically dissociated in CMF-HBSS containing 0.125% trypsin at 37 °C for 15 min. Then the digestion was terminated with DMEM/F12 (1:1) containing 10% FBS (Gibico) and tissues were triturated with a fire-polished glass pipet. Dispersed cells were diluted with DMEM/F12 (1:1) containing 10% FBS and 1% streptomycin/penicillin and seeded at 5×10^4 cells/cm^2 on dishes coated with 10 μg/mL polyornithine (Sigma−Aldrich). The medium was replaced every 2−3 days.

2.9.4. Oxygen and glucose deprivation

Cultured neurons (Day 14 *in vitro*) or glia (90% confluence) were exposed to 2 h of OGD as previously[45]. Briefly, cultures were rinsed twice with serum- and glucose-free medium and incubated with serum- and glucose-free medium in a hypoxia chamber (MACS MICS jar gassing system, Don Whitley Scientific). The chamber was flushed with a mixture of 85% N_2, 10% H_2 and 5% CO_2 through 2 anaerobic cycles, and then sealed and maintained at 37 °C for 2 h. After OGD, the serum- and glucose-free medium was replaced with normal medium and the cultures were returned back to normoxic incubator.

2.10. Slice preparation for electrophysiology

Mice were sacrificed between 12 and 24 h after ischemia surgery or on Days 14−21 after AAVs microinjection and brain slices were prepared[41,43]. Under deep ethyl ether anesthesia, mice were decapitated. Brains were quickly removed and placed into ice-cold buffer containing 110 mmol/L choline chloride, 20 mmol/L glucose, 2.5 mmol/L KCl, 0.5 mmol/L $CaCl_2$, 7 mmol/L $MgCl_2$, 1.3 mmol/L NaH_2PO_4, 25 mmol/L $NaHCO_3$, 1.3 mmol/L Na-ascorbate, 0.6 mmol/L Na-pyruvate. Brains were vibratome-sectioned in the same solution at 350 μm and transferred to an interface-style chamber containing artificial cerebrospinal fluid (aCSF) composed of 10 mmol/L glucose, 125 mmol/L NaCl, 2.5 mmol/L KCl, 2 mmol/L $CaCl_2$, 1.3 mmol/L $MgCl_2$, 1.3 mmol/L NaH_2PO_4, 25 mmol/L $NaHCO_3$, 1.3 mmol/L Na-ascorbate, 0.6 mmol/L Na-pyruvate (pH 7.4). Slices were recovered at 34 °C for at least 1 h before recording. All solution was gassed with 95% O_2 and 5% CO_2.

2.11. Electrophysiological recordings

Brain slices from mice receiving different treatments (AAVs-infected and/or PT-exposed) or HEK293 cells transfected with desired plasmid were transferred to a recording chamber that was continuously perfused with oxygenated aCSF (flow rate, 4−6 mL/min). The slices were visualized using an upright microscope (Olympus X51W, Nomasky) with a 5 × 0.1 NA or 60 × 1.0 NA objective and infrared and differential interference contrast optics. The fluorescent cells were visualized under an Olympus X51W microscope equipped with a 60 × water-immersion lens and illuminated with a mercury lamp. For brain slices, whole-cell recordings were made in layer V pyramidal neurons within AAVs-infected peri-infarct cortex (< 400 μm from the infarct) or corresponding locations in sham-operated mice 12−24 h after ischemia surgery. For HEK293 cells, whole-cell recordings were made in GFP-labeled cells within 22−30 h after plasmids transfection. All recordings used patch-clamp electrodes and were low-pass filtered at 2 kHz and sampled at 10 kHz using a digitizer (Digidata 1440A, Axon Instruments). Access resistance was 5−25 MΩ and was monitored throughout the experiment (neurons with access resistance changes > 20% were excluded). Data were collected with pClamp 10.3 software and analyed using Clampfit 10.3 (Molecular Devices). Spontaneous EPSCs (for tonic excitation), miniature EPSCs, voltage-dependent currents of Cl^- channel (for I−V curve) and anoxic depolarization (AD) currents were recorded on layer V pyramidal neurons in the peri-infarct cortex. Voltage-dependent currents of Cl^- channel (for I−V curve) were recorded on HEK293 cells. All experiments were performed by a researcher blinded to group allocation.

2.11.1. Glutamate tonic excitation

To determine the level of tonic excitation resulted from extrasynaptic glutamate release, we monitored the shift in holding current (baseline) of spontaneous EPSCs (sEPSCs) in brain slices before and after NPPB (100 μmol/L) application in bath solution[26,47,48]. Patch electrodes (4-6 MΩ) were filled with pipette solution containing (in mmol/L): 132.5 Cs-gluconate, 17.5 CsCl, 2 $MgCl_2$, 0.5 EGTA, 10 HEPES, 4 ATP, 5 QX-314 (pH 7.3). For voltage-clamp recordings, sEPSCs were recorded at −60 mV. All recordings were performed in the presence of 20 μmol/L BMI in the bath solution aCSF to isolate glutamate-mediated currents. Low Mg^{2+} aCSF (20 μmol/L $MgCl_2$) was used to facilitate measurements of NMDA-mediated currents. Baseline shift of sEPSCs was regarded as change of tonic excitation currents (ΔI_{tonic}). For ion substitution experiments, a low external Cl^- concentration was acquired by replacing 125 mmol/L NaCl with 125 mmol/L Na-gluconate in aCSF.

2.11.2. mEPSCs

Miniature EPSCs (mEPSCs) were recorded the same as sEPSCs, except that tetrodotoxin (0.5 μmol/L) was added to block action potentials. The recording was more than 5 min. Amplitude and frequency of sEPSCs were analyzed with Mini software (Synaptosoft Inc. Fort Lee, NJ, USA). Up to 100 events from each neuron were selected at a fixed sampling interval to generate cumulative probability.

2.11.3. AD currents

Anoxic depolarization (AD) currents in brain slices were induced by oxygen and glucose deprivation (OGD) and recorded as reported[25]. Voltage-clamp recording pipettes (4−6 MΩ) were filled with a solution containing 135 mmol/L CsCl, 4 mmol/L NaCl, 0.7 mmol/L $CaCl_2$, 10 mmol/L BAPTA, 10 mmol/L HEPES, 4 mmol/L Mg-ATP, and 0.5 mmol/L Na_2-GTP (pH 7.3). All AD currents were recorded in the presence of BMI (20 μmol/L) to block GABA receptors. To simulate ischemia, glucose in bath solution aCSF was replaced with 10 mmol/L sucrose, and 95% O_2/5% CO_2 was replaced with 95% N_2/5% CO_2. Cells were held at −30 mV to facilitate the sensing of ischemia-evoked currents through NMDARs. AP-5 (50 μmol/L) and CNQX (10 μmol/L) were applied concomitantly with ischemia stimulation.

2.11.4. I−V curve

Voltage-dependent currents of Cl^- channel were recorded on brain slices or HEK293 cells as reported[33]. The recording pipettes (4−6 MΩ) were filled with a solution containing (in mmol/L): 146 CsCl, 5 $CaCl_2$, 5 EGTA (ethylene glycol tetraacetic acid)-NMDG (free calcium concentration approximately 4.5 μmol/L), 2 $MgCl_2$, 10 HEPES, 10 sucrose, 4 Mg-ATP, and 0.3 Na_2-GTP (pH 7.3). For brain slice recordings, aCSF was used as the external solution; For HEK293 cell recordings, the external solution contained (in mmol/L): 150 NaCl, 10 HEPES, 3 KCl, 2 $CaCl_2$, 2 $MgCl_2$, 5.5 glucose. To measure the glutamate permeability of BEST1 channel, 146 mmol/L CsCl in the pipette solution was replaced with 146 mmol/L CsGlutamate. CsGlutamate was achieved by equimolar of CsOH and glutamic acid. From a holding potential of −70 or 0 mV (as indicated), the voltage was stepped between −100 and + 100 mV, in 20-mV increments, and I−V curve was established.

2.12. Microdialysis and UPLC−MS/MS analysis

Microdialysis was performed in the peri-infarct cortex within 12−24 h after PT surgery and the concentrations of GABA and glutamate in dialysates were analyzed using UPLC−MS/MS as described previously[27,49].

2.12.1. Microdialysis in vivo

Microdialysis in the peri-infarct cortex was performed within 12−24 h after PT surgery as reported previously with some modifications[27]. Briefly, mice were kept under isoflurane anesthesia (1.5%) and mounted in a stereotaxic frame (Kopf). After exposing the skull and drilling a burr hole, a CMA7 microdialysis probe of concentric design (CMA Microdialysis) was positioned and inserted into the peri-infarct area with the following coordinates (from bregma): anteroposterior, 0 mm; mediolateral, −1.0 mm; dorsoventral, 1.0 mm. The probe was connected to a 100 μL microsyringe (Hamilton) controlled by a microperfusion pump (WPI) with polyethylene (PE-20) and perfused with aSCF composed of the following (in mmol/L): 10 mmol/L glucose, 125 mmol/L NaCl, 2.5 mmol/L KCl, 2 mmol/L $CaCl_2$, 1.3 mmol/L $MgCl_2$, 1.3 mmol/L NaH_2PO_4, 25 mmol/L $NaHCO_3$ at a speed of 1 L/min. Perfusates from the outlet end of the tubing were collected in plastic vials standing on ice. Samples were collected over 1 h (20 μL/20 min for each dialysate, 3 consecutive dialysates for 1 mouse). The second dialysate was used for concentration measurement of L-glutamate and GABA.

2.12.2. UPLC−MS/MS analysis

After an orthogonal dansyl-labeling and label-free dual pretreatment[49], samples were analyzed using a QTRAP 5500 mass spectrometer (AB Sciex, Foster City, CA, USA) linked to an Ultra Performance LC system (AB Sciex). The chromatographic separation was realized on Waters ACQUITY UPLC HSS T3 Column

(2.1 mm × 150 mm, 1.8 μm). MRM monitoring conditions for each compound were performed on Analyst R914.6.2 (AB Sciex). The parameters of mass spectrometer were summarized as follows: ion spray voltage, +5.5 kV; temperature, 50 °C; curtain gas, 35 psi entrance potential, 10.0 V; collision cell exit potential: 13.0 V. Data acquisition and analysis were performed on Analyst R914.6.2 software (AB Sciex).

2.13. Statistical analysis

The accurate sample size is given in each figure and legend. For biochemical measurements and electrophysiological recordings, no data were excluded from the analysis unless the data were not successfully obtained for technical or accidental reasons. For behavioral tests, animals were excluded from the analysis if accidental events occurred, such as escape and no movement in tests. The data from the mice whose brain region was not been correctly targeted in microinjection were also excluded. The details of excluded animals, if any, are provided in each figure legend.

Appropriate parametric statistics were utilized to test our hypothesis. Comparisons among multiple groups were made by Tukey's *post hoc* test following one-way or two-way ANOVA, and comparisons between two groups were made by Sidak's *post hoc* test following two-way ANOVA, according to the recommendation of GraphPad Prism 6 software (GraphPad Software, RRID: SCR_002798). *Post hoc* test was performed only when ANOVA yielded a significant main effect. Comparisons between the two groups were made with unpaired two-tailed Student's *t*-test (GraphPad Prism 6 software). Cumulative probability plots were produced for the analysis of mEPSCs with Mini Analysis software 6.0 (Synaptosoft, RRID: SCR_002184), and statistical analysis was performed on mean values. Data are presented as the mean ± standard error of mean (SEM), and $P < 0.05$ was considered statistically significant.

3. Results

3.1. Increased BEST1 expression is involved in the deterioration of acute ischemic damage

We examined the protein expression of BEST1 within the peri-infarct cortex of mice after photothrombotic ischemia (PT). As shown in Fig. 1A, BEST1 expression increased from 8 h to 48 h after ischemia, with a peak (approximately 4-fold as the level of sham) at 12−24 h ($F_{(5,24)} = 10.89$, $P = 0.003$ for 8 h, < 0.001 for 12 and 24 h, $= 0.003$ for 48 h). To determine whether the increased BEST1 was involved in the expansion of acute ischemic damage, we generated a recombinant adeno-associated virus AAV-CMV-sh*Best1*-GFP that contained mouse *Best1*-targeting shRNA. AAV-CMV-sh*Best1*-GFP or its control AAV-CMV-GFP was microinjected into the right motor cortex of mice and the PT stroke was induced at the same location of the cortex 14 days later (Fig. 1B). AAV-CMV-sh*Best1*-GFP could effectively infected the peri-infarct cortex (Fig. 1C) and steadily knockdown the expression of BEST1 (Fig. 1D and E, $F_{(3,12)} = 27.73$, $P < 0.001$). Then, we performed the behavioral tests. On Day 3 after PT, ischemia led to an increase in the forelimb asymmetry index in the cylinder task (Fig. 1F) and an increase in the number of left forelimb foot faults in the grid-walking task (Fig. 1G), indicating the damaged motor functions of left forelimb. AAV-CMV-sh*Best1*-GFP produced a functional improvement of the left forelimb compared to AAV-CMV-GFP in both tasks (Fig. 1F, $F_{(3,52)} = 20.75$, $P < 0.001$; Fig. 1G, $F_{(3,52)} = 20.33$, $P < 0.001$), without significant influences on the motor function of the right forelimb (Fig. 1H). The mice infected with AAV-CMV-sh*Best1*-GFP showed a tendency of lower infarct volume than those infected with AAV-CMV-GFP (Fig. 1I and J, $F_{(3,52)} = 3.945$, $P = 0.266$). Furthermore, we confirmed the protective effects of BEST1 knockdown with a mouse model of middle cerebral artery occlusion (MCAO) (Supporting Information Fig. S1A). AAV-CMV-sh*Best1*-GFP was microinjected 14 days before MCAO at 3 sites within the right hemisphere to obtain a wide infection in the cortex (Fig. S1B). Two days after MCAO, neurological deficits and infarct volume were evaluated. The results show that sh*Best1* treatment significantly decreased the score of neurological deficits (Fig. S1C, $F_{(3,41)} = 31.11$, $P = 0.004$) and the infarct volume (Fig. S1D and S1E, $F_{(3,41)} = 40.22$, $P = 0.0096$). Thus, the findings reveal that preventing the enhancement of BEST1 expression after cerebral ischemia reduces the deterioration of acute ischemic damage.

3.2. Neuron-specific knockdown of BEST1 alleviates functional loss

It is reported that BEST1 is widely distributed in mice brain and expressed in both astrocytes and neurons[32], however, the cell type responding to the ischemic damage is not known. We labeled the peri-infarct cortex with BEST1, NeuN and GFAP antibodies at 12 h after PT, and found that the expression of BEST1 was prominently augmented in neurons while astrocytes were not yet activated and the BEST1 expression in astrocytes was not obvious within 48 h post PT (Supporting Information Fig. S2A). *In vitro*, cultured cortex neurons but not glia showed a significant increase of BEST1 expression level after exposure to oxygen−glucose deprivation (OGD) (Fig. S2B−S2E). To further confirm the role of neuronal BEST1 in acute ischemic damage, we combined AAV-Syn-Cre and AAV-Flex-sh*Best1*-GFP to knock down the BEST1 expression in neurons specifically (Fig. 2A). The mixed AAVs effectively infected the peri-infarct cortex and GFP fluorescence indicated the Cre-dependent recombination (Fig. 2B). Importantly, the Cre-dependent GFP expression was found mainly in neurons (approximately 87% for GFP^+&$NeuN^+$/GFP^+ and 2% for GFP^+&$GFAP^+$/GFP^+). Compared to control, sh*Best1* led to the dramatic decline of the $BEST1^+$ neurons ($BEST1^+$&$NeuN^+$/$NeuN^+$, Fig. 2C and D, $t_{10} = 14.52$, $P < 0.001$), without any significant influence on the $BEST1^+$ astrocytes ($BEST1^+$&$GFAP^+$/$GFAP^+$, Fig. 2C and D, $t_{10} = 0.2868$, $P = 0.780$), confirming the effective and specific knockdown of BEST1 in neurons. We also evaluated the motor functions on Day 3 after PT. As expected, the mice in Syn-Cre + Flex-sh*Best1*-GFP group showed smaller forelimb asymmetry index (Fig. 2E, $F_{(3,51)} = 29.46$, $P < 0.001$) and less left forelimb foot faults ratio (Fig. 2F, $F_{(3,51)} = 24.16$, $P < 0.001$), compared with the mice in Syn-Cre + Flex-GFP group. Meanwhile, the mice in different groups made similar right forelimb foot faults (Fig. 2G). The behavioral tests demonstrate that neuron-specific knockdown of *BEST1* by combination of AAV-Syn-Cre and AAV-Flex-sh*Best1*-GFP alleviates the motor function impairment induced by PT stroke. Consistently, neuron-specific knockdown of BEST1 in mice resulted in a tendency of lower infarct volume (Fig. 2H, $F_{(3,51)} = 70.56$, $P = 0.270$).

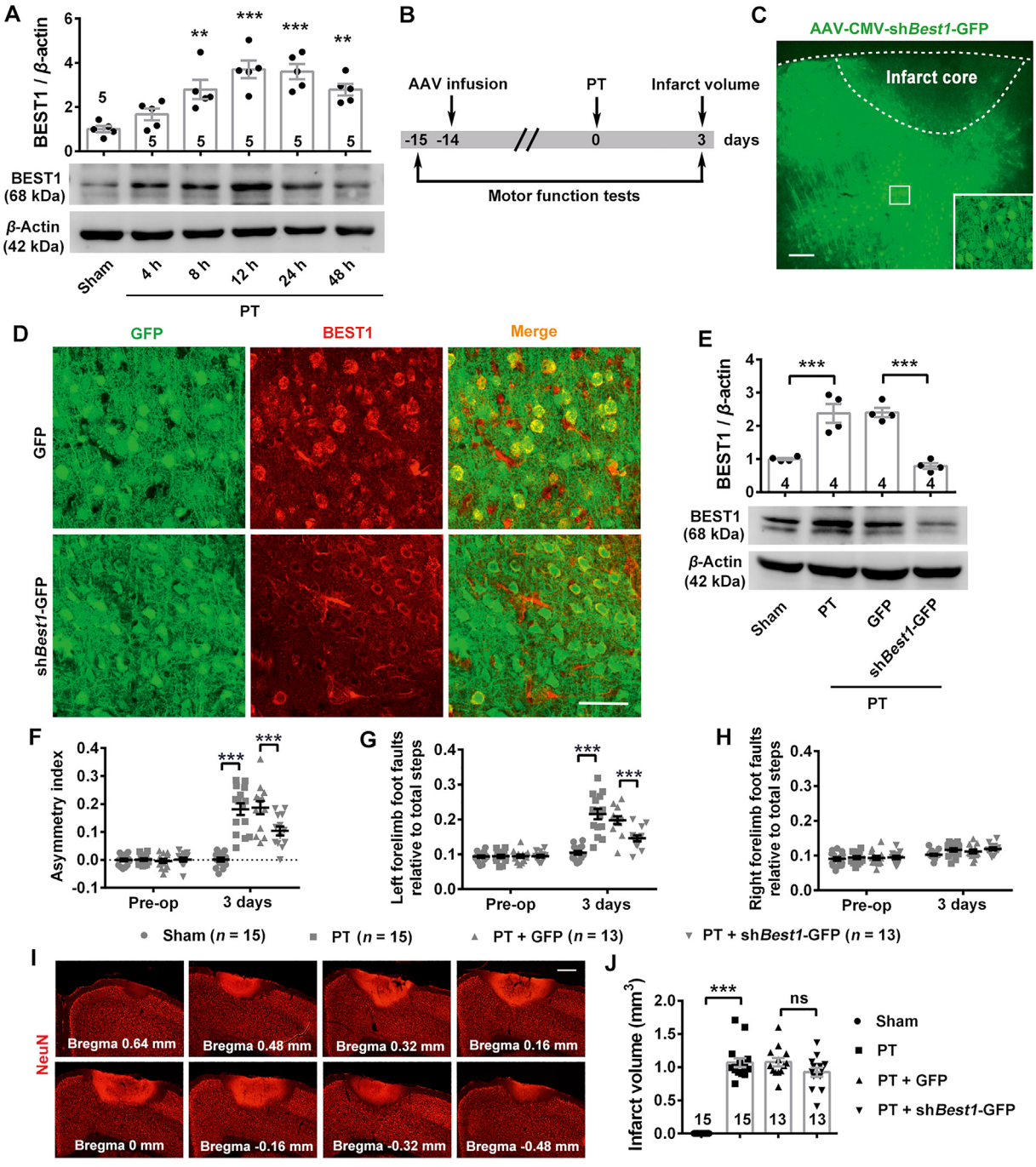

Figure 1 The role of BEST1 in PT-induced acute ischemic damage. (A) Scatter plot (top, $n = 5$) and representative blots (bottom) showing the time course of BEST1 expression in the peri-infarct cortex after PT. (B) The scheme of experimental design. (C) Representative fluorescence image showing sh*Best1*-GFP expression in the peri-infarct cortex of mice infected with AAV-CMV-sh*Best1*-GFP 3 days after PT. Similar results were observed with 3 mice. (D, E) Representative fluorescence images (D) and Western blots (E, $n = 4$) showing BEST1 expression in the mice infected with AAV-CMV-GFP or AAV-CMV-sh*Best1*-GFP 3 days after PT. (F–H) Scatter plots showing forelimb asymmetry (F) in cylinder task, foot faults of left (G) and right (H) forelimb in grid-walking task for mice in 4 groups: sham, PT, PT + GFP (injected with AAV-CMV-GFP) and PT + sh*Best1*-GFP (injected with AAV-CMV-sh*Best1*-GFP). $n = 13-15$. Two mice in PT + GFP group and two mice in PT + sh*Best1*-GFP group were excluded because the brain region was not correctly targeted in microinjection. (I, J) Representative immunofluorescence images (I) and scatter plot (J) showing infarct volume on Day 3 after PT surgery. $n = 13-15$. Data are mean ± SEM; $^{**}P < 0.01$, $^{***}P < 0.001$, ns = no significance, compared with sham in (A). Scale bars, 100 μm in (C), 50 μm in (D), and 400 μm in (I).

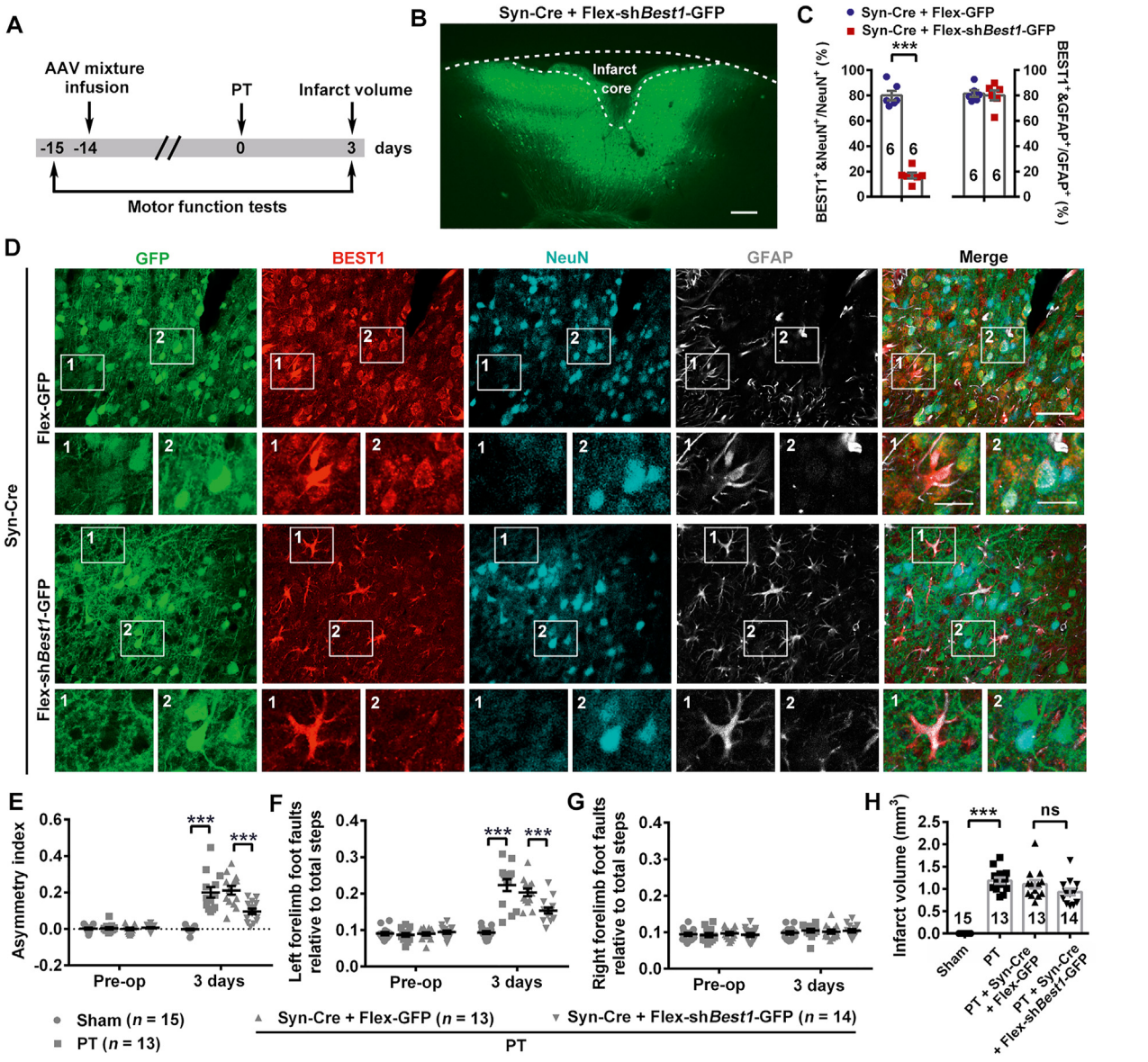

Figure 2 The effects of neuron-specific knockdown of BEST1 against PT ischemia. (A) The scheme of experimental design. (B) Representative fluorescence image showing sh*Best1*-GFP expression in the peri-infarct cortex of mice infected with mixed AAV-Syn-Cre and AAV-Flex-sh*Best1*-GFP 4 days after PT. Similar results were observed with 4 mice. (C) Scatter plot showing the ratio of BEST1$^+$ neurons and BEST1$^+$ astrocytes in mice infected with AAV-Syn-Cre + AAV-Flex-sh*Best1*-GFP or AAV-Syn-Cre + AAV-Flex-GFP 4 days after PT. $n = 6$. (D) Representative fluorescence images showing specific knockdown of BEST1 expression in neurons by the combination of AAV-Syn-Cre and AAV-Flex-sh*Best1*-GFP. Similar results were observed with 3 mice. (E−G) Scatter plots showing forelimb asymmetry (E) in cylinder task, foot faults of left (F) and right (G) forelimb in grid-walking task for mice in 4 groups: sham, PT, PT + Syn-Cre + Flex-GFP (infused with mixed AAV-Syn-Cre and AAV-Flex-GFP) and PT + Syn-Cre + Flex-sh*Best1*-GFP (infused with mixed AAV-Syn-Cre and AAV-Flex-sh*Best1*-GFP). $n = 13$−15. One mouse in PT + Syn-Cre + Flex-GFP group and one mouse in PT + Syn-Cre + Flex-sh*Best1*-GFP group were excluded because brain region was not correctly targeted in microinjection. Two mice in PT group and one mouse in PT + Syn-Cre + Flex-GFP group were excluded because of no movement in tests. (H) Scatter plot showing infarct volume assessed by NeuN-labeling on Day 3 after PT surgery. $n = 13$−15. Data are mean ± SEM; ***$P < 0.001$, ns = no significance. Scale bars, 200 μm in (B), 50 μm in (D) (top) and 20 μm in (D) (left bottom and right bottom).

3.3. *Knockdown of neuronal BEST1 shows neuroprotective effects*

As shown in Fig. 3A and B, on Day 3 after PT stroke, only ~1/4 neurons survived (PT *vs.* Sham, $F_{(3,20)} = 212.1$, $P < 0.001$) in the peri-infarct cortex and neuron-specific knockdown of BEST1 partly rescued the loss of NeuN$^+$ cells (PT + Syn-Cre + Flex-sh*Best1*-GFP *vs.* PT + Syn-Cre + Flex-GFP, $F_{(3,20)} = 212.1$, $P < 0.001$). Moreover, the PT-induced decrease of miniature excitatory post-synaptic currents (mEPSCs) frequency recorded on brain slices was markedly alleviated by neuron-specific knockdown of BEST1 (Fig. 3C−E, $F_{(3,44)} = 8.833$, $P = 0.010$,

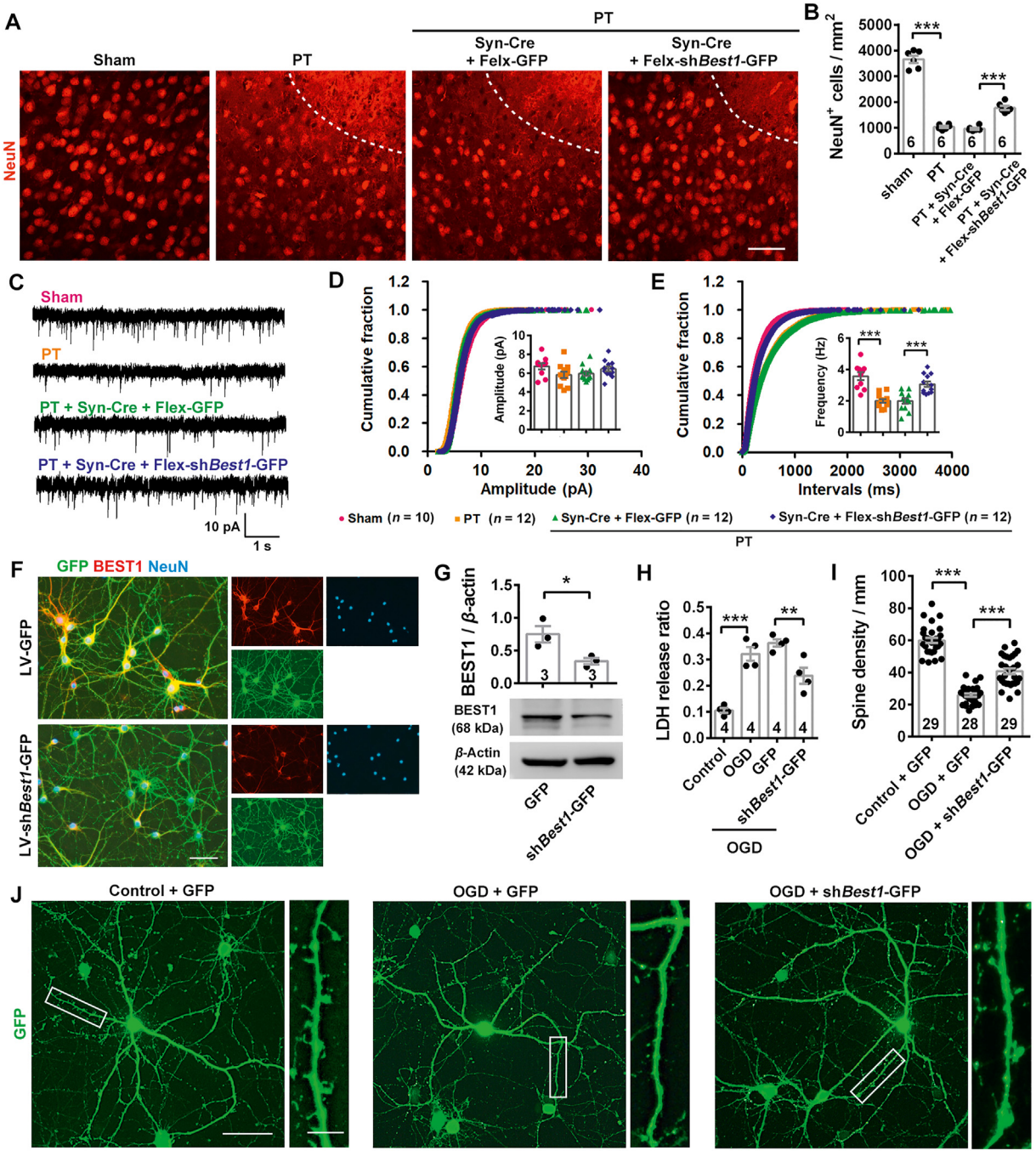

Figure 3 The neuroprotection of BEST1 knockdown in neurons. (A, B) Representative immunofluorescence images (A) and scatter plot (B, $n = 6$) showing the number of NeuN$^+$ cells in the peri-infarct cortex. (C) Representative traces of mEPSCs recorded on pyramidal neurons in the peri-infarct cortex (or the corresponding location) on Day 3 after PT (or sham) surgery. (D, E) Cumulative fraction plots of mEPSC amplitude (D, mean amplitude in inset) and interevent intervals (E, mean frequency in inset). $n = 10-12$ neurons (from 5 to 6 mice). The mixed AAV-Syn-Cre and AAV-Flex-sh*Best1*-GFP (or AAV-Flex-GFP) was microinjected 14 days before PT surgery. (F–J) Representative immunofluorescence images (F) and scatter plot for Western blot (G, $n = 3$) showing BEST1 expression of cultured cortex primary neurons infected with LV-CMV-sh*Best1*-GFP or it control LV-CMV-GFP at day 14 *in vitro*. (H) Scatter plot showing LDH release ratio of cultured neurons during 8–24 h after OGD exposure. $n = 4$ (from 2 independent experiments). (I, J) Scatter plot (I) and representative immunofluorescence images (J) showing the spine density of cultured neurons 24 h after OGD exposure. $n = 28-29$ neurons from 3 independent experiments. Neurons in Control + GFP, OGD + GFP and OGD + sh*Best1*-GFP group were infected with LV-CMV-GFP, LV-CMV-GFP, and LV-CMV-sh*Best1*-GFP, respectively. Data are mean ± SEM; $^*P < 0.05$, $^{**}P < 0.01$, $^{***}P < 0.001$. Scale bars, 50 μm in (A, F, and J) (left), 10 μm in (J) (right).

PT + Syn-Cre + Flex-sh*Best1*-GFP *vs.* PT + Syn-Cre + Flex-GFP), suggesting the reversed impairment of synaptic transmission accompanied with reduced neuronal damage. No significant difference in the amplitude of mEPSCs was observed. Moreover, mice infected with Syn-Cre and Flex-sh*Best1*-GFP showed a higher expression of synapse-associated proteins (synapsin and PSD-95) in the peri-infarct cortex than mice infected with Syn-Cre and Flex-GFP (Supporting Information Fig. S3A). To further confirm the neuroprotection of neuron-specific knockdown of BEST1 observed in mice, we generated a recombinant lentivirus LV-CMV-sh*Best1*-GFP to interfere with the BEST1 expression in cultured primary cortex neurons exposed to OGD *in vitro*. LV-CMV-sh*Best1*-GFP infected most of the cultured neurons (~92%, Fig. 3F) and produced a substantial reduction of BEST1 expression (Fig. 3F and G, $t_4 = 3.073$, $P = 0.037$). Effective knockdown of BEST1 in LV-CMV-sh*Best1*-GFP-infected neurons led to smaller LDH release ratio (Fig. 3H, $F_{(3,12)} = 26.70$, $P = 0.008$), greater spine density (Fig. 3I and J, $F_{(2,83)} = 125.0$, $P < 0.001$) and more synapsin$^+$&PSD-95$^+$ puncta (Fig. S3B and S3C, $F_{(2,86)} = 270.0$, $P < 0.001$) after exposure to OGD, compared with LV-CMV-GFP-infected neurons. Therefore, OGD-induced neuronal damage was ameliorated partly but significantly by sh*Best1*, in agreement with the neuroprotection found in animal experiment.

3.4. *BEST1-mediated ischemic damage is due to enhanced channel function*

As BEST1 is a member of CaCCs[30], there is a great possibility that enhanced channel function contributes to the deterioration of acute ischemic damage mediated by BEST1. We then observed the current-voltage relationship of CaCCs in peri-infarct cortex neurons 12−24 h after PT with the whole-cell voltage patch (stepped form −100 mV to +100 mV). As expected, the voltage-dependent currents increased in PT mice, compared to sham mice (Fig. 4A and B, $F_{(3,36)} = 34.56$, $P < 0.001$). This current was almost not observed in the complete absence of internal Ca^{2+}, and was very small in the presence of an Cl^- channel blocker, 5-nitro-2-(3-phenylpropylamino) benzoic acid (NPPB) (Fig. 4A and B, $F_{(3,36)} = 34.56$, $P < 0.001$). Moreover, the reversal potential was +3.9 ± 0.8 mV, which closely matched the equilibrium potential of +4.5 mV estimated for Cl^- under these experimental conditions. Thus, the permeability of BEST1 channel could be enhanced along with ischemia-induced BEST1 expression. This speculation was further supported by the evidence that BEST1 knockdown obviously suppressed the voltage-dependent CaCC currents under ischemic condition (Fig. 4C and D, $t_{18} = 7.00$, $P < 0.001$). These electrophysiological results indicate the strengthened BEST1 channel function and increased permeability of Cl^- through BEST1 after acute ischemia.

To determine whether the BEST1 channel function was implicated in ischemia-impaired motor function, we constructed AAV-CMV-BEST1^{W93C}-3Flag-T2A-GFP, which expressed a mutant of BEST1 (tryptophan-93 to cysteine-93). This anion-selective pore mutation has been proved to impair the CaCC currents for BEST1[32,42]. Consistently, we also found that BEST1^{W93C}-expressing HEK293 cells did not show any significant CaCC current when the voltage was stepped between −100 and + 100 mV, although BEST1^{WT}-expressing HEK293 cells did, with a high Ca^{2+}-containing pipette internal solution (Supporting Information Fig. S4A−S4C). Then we infused AAV-CMV-BEST1^{W93C}-3Flag-T2A-GFP or its control AAV-CMV-3Flag-T2A-GFP into the motor cortex of mice before PT surgery and measured the animal motor functions as illustrated in Fig. 1B. With effective expression in the neurons of peri-infarct cortex (Fig. 4E), BEST1^{W93C} could significantly reduce the left forelimb motor function impairments of PT mice in both the cylinder task (Fig. 4F, $F_{(3,53)} = 37.31$, $P < 0.001$) and the grid-walking task (Fig. 4G, $F_{(3,53)} = 12.82$, $P < 0.001$). There was no difference in right forelimb motor function among groups (Fig. 4H). Together, the above data suggest that strengthened CaCC function after enhanced BEST1 expression accounts for BEST1-mediated ischemic damage.

3.5. *Upregulated BEST1 contributes to aberrant glutamate release*

In addition to conducting Cl^-, the most prominent feature of astrocytic BEST1 is its significant permeability to glutamate and GABA[33−35]. Next, we tested whether glutamate or GABA release was increased along with upregulation of neuronal BEST1. UPLC−MS/MS analysis following microdialysis revealed that during 12−24 h after PT stroke when BEST1 was highly expressed in neurons, the extracellular glutamate concentration in the peri-infarct cortex was nearly 4-fold high as the level of sham (Fig. 5A and B, $F_{(3,18)} = 7.661$, $P = 0.040$), which began to increase from 6 h (though without significant difference) and still markedly elevated at 48 h after PT stroke (Supporting Information Fig. S5), indicating a delayed peak of glutamate release after the well-known acute glutamate release happening 1−2 h after stroke onset. BEST1 knockdown completely inhibited this delayed elevation of extracellular glutamate concentration (Fig. 5A and B, $F_{(3,18)} = 7.661$, $P = 0.007$). Meanwhile, the extracellular GABA concentration was not substantially changed by BEST1 knockdown (Fig. 5C and D, $F_{(3,18)} = 0.806$, $P = 0.993$). It is likely that BEST1 facilitates glutamate release when its expression is induced after PT stroke. Then we recorded mEPSCs in the peri-infarct cortex during the same time period to reflect the excitatory synaptic transmission. Surprisingly, either amplitude or frequency of mEPSCs remained similar whenever BEST1 was knocked down or not (Supporting Information Fig. S6A−S6C), indicating that synaptic glutamate vesicle exocytosis was not influenced by BEST1 even though the expression and function of BEST1 was enhanced after ischemia. Therefore, the possible BEST1-associated glutamate release was through an extrasynaptic mechanism. This was further supported by the following recordings of the tonic excitatory activity on peri-infarct cortex neurons. Consistent with the previous report[26,47,48], we observed an outward shift in the holding current of sEPSCs after the combinational application of AP-5 and CNQX to block ionotropic glutamate receptors (Supporting Information Fig. S7A), which represented the level of tonic excitation resulted from extrasynaptic glutamate release. In agreement with the elevated extracellular glutamate concentration, PT group showed a higher level of tonic excitation than sham group 12−24 h after ischemia (Supporting Information Fig. S7A and S8B, $t_{11} = 10.65$, $P < 0.001$), which was not due to NMDARs expression alteration, because GluN2B-containing NMDARs, the main NMDAR isoform locating at extrasynaptic sites, maintained relatively stable expression in peri-infarct cortex after PT (Supporting Information Fig. S8A and S8B). Moreover, the contribution of the SWELL1 channel to the increase of tonic excitation was not significant, because the application of a blocker of volume-regulated anion channel, 4-(2-butyl-6,7-dichloro-2-cyclopentyl-indan-1-on-5-yl)

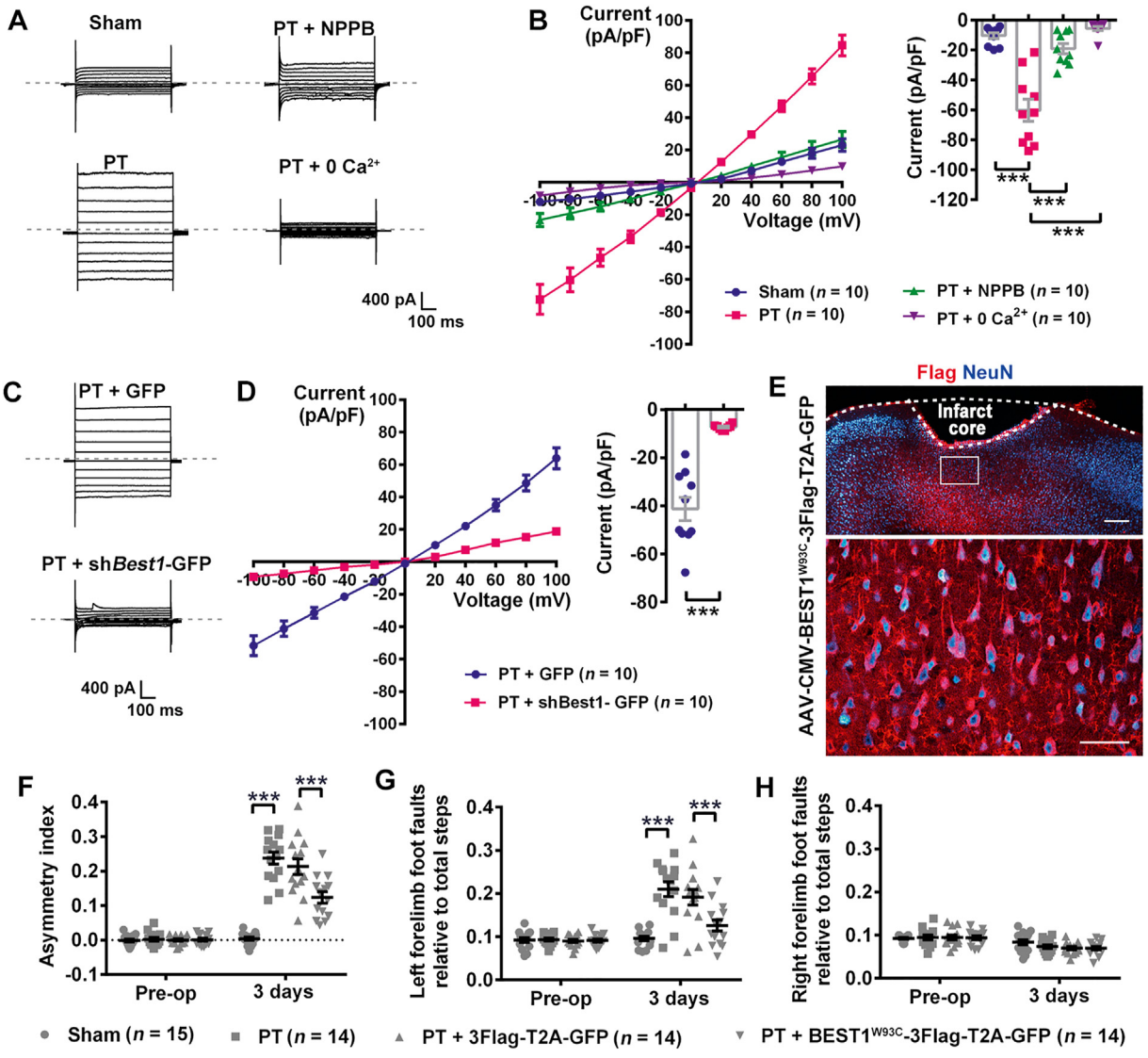

Figure 4 The contribution of BEST1 channel permeability to acute ischemia-impaired motor function. (A) Representative current traces were recorded with whole-cell patch-clamp on pyramidal neurons of the peri-infarct cortex 12−24 h after PT or sham surgery. Internal solution for all groups contained ~4.5 μmol/L Ca^{2+}, except 0 Ca^{2+} group. For NPPB group, 100 μmol/L NPPB was contained in external solution. (B) Current-voltage curves (left) and current amplitudes at −80 mV (right) for the recordings shown in (A). $n = 10$ neurons (from 4 to 5 mice). (C) Representative current traces recorded on pyramidal neurons in peri-infarct cortex of AAV-CMV-sh*Best1*-GFP- or AAV-CMV-GFP-infected PT mice. AAV-CMV-sh*Best1*-GFP or AAV-CMV-GFP was microinjected 14 days before ischemic surgery, and the whole-cell patch-clamp was recorded 12−24 h after surgery. (D) Current-voltage curves (left) and current amplitudes at −80 mV (right) for the recordings shown in C. $n = 10$ neurons (from 4 to 5 mice). (E) Representative immunofluorescence images showing effective $BEST1^{W93C}$-3Flag expression in the neurons in peri-infarct cortex of mice infected with AAV-CMV-$BEST1^{W93C}$-3Flag-T2A-GFP 3 days after PT. Similar results were observed with 4 mice. (F−H) Scatter plots showing forelimb asymmetry (F) in cylinder task, foot faults of left (G) and right (H) forelimb in grid-walking task for mice in 4 groups: sham, PT, PT+3Flag-T2A-GFP (infused with AAV-CMV-3Flag-T2A-GFP) and PT + $BEST1^{W93C}$-3Flag-T2A-GFP (infused with AAV-CMV-$BEST1^{W93C}$-3Flag-T2A-GFP). $n = 14$−15. One mouse in each group except sham group was excluded because of no movement in tests. Data are mean ± SEM; $^{***}P < 0.001$. Scale bars, 200 μm in (E) (top) and 50 μm in (E) (bottom).

oxobutyric acid (DCPIB), produced similarly slight reduction of the tonic excitation in sham and PT groups (Fig. 5E and F). The contribution of excitatory amino acid transporters (EAATs) was also excluded, because the application of a broad-spectrum non-substrate antagonist of EAATs, D,L-threo-β-benzyloxyaspartic acid (TBOA), did not reduce the tonic excitation but augmented it in both sham and PT groups with similar degree (Fig. 5G and H), implying that 12−24 h after ischemia, most transporters worked in direct uptake mode as they did under physiological condition. In agreement with the similar effect of TBOA on tonic excitation in sham and PT group, the expression of GLT-1, one of the most important EAATs for extracellular glutamate homeostasis, in peri-infarct cortex did not show significant changes during 12−24 h after PT (Fig. S8A and S8C). Then we employed NPPB to block BEST1 channel. NPPB only produced a slight reduction of the tonic excitation when applied to slices from sham mice, but led to

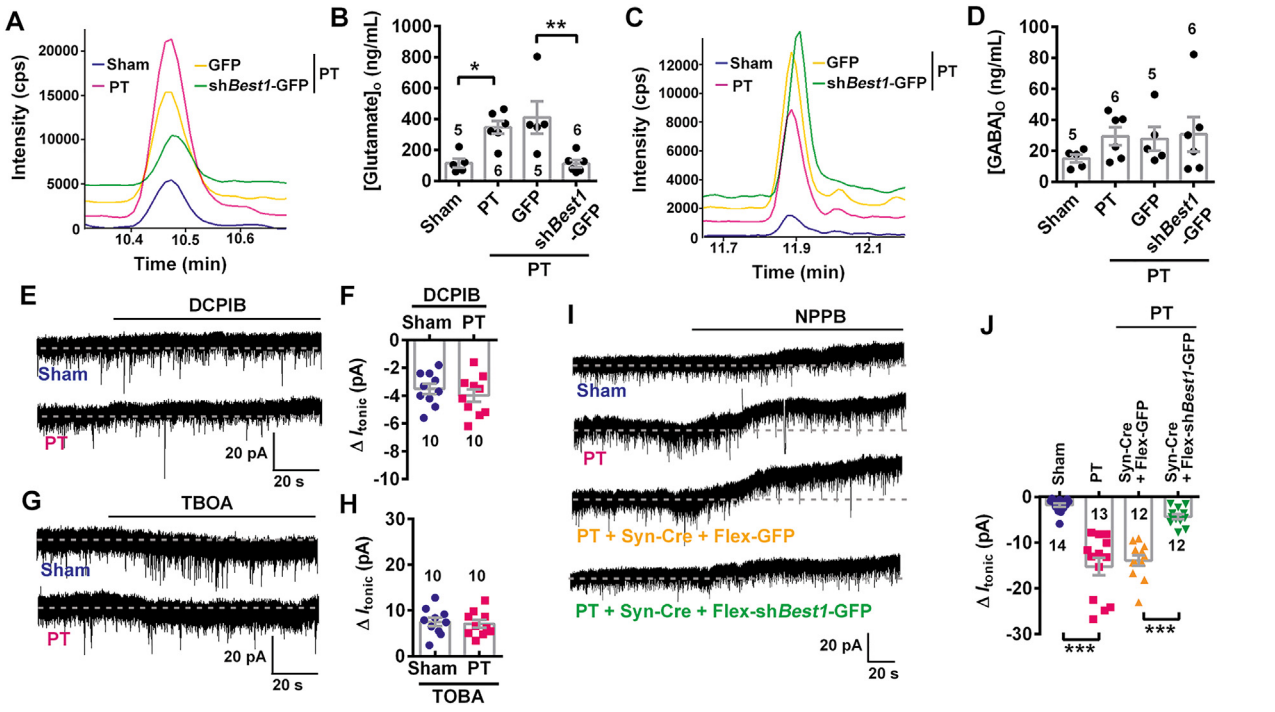

Figure 5 BEST1-mediated extrasynaptic glutamate release. (A−D) Characteristic peaks of glutamate (A) and GABA (C) from ion flow chromatograph by UPLC−MS/MS and scatter plots showing extracellular glutamate (B) and GABA (D) concentration by microdialysis. AAV-CMV-sh*Best1*-GFP or AAV-CMV-GFP was microinjected 14 days before PT surgery, and dialysate was collected 12−24 h after surgery. $n = 5$−6. (E−H) Representative traces of sEPSCs with baseline shift (E and G) and scatter plot (F and H) showing the change of glutamate tonic excitation after DCPIB (50 μmol/L) or TBOA (30 μmol/L) application. Whole-cell currents were recorded on the pyramidal neurons of peri-infarct cortex (or the corresponding location) during 12−24 h after PT (or sham) surgery. $n = 10$ neurons (from 4 mice). (I, J) Representative traces of sEPSCs with baseline shift (I) and scatter plot (J) showing the change of glutamate tonic excitation after NPPB (100 μmol/L) application in PT (or sham) mice. The mice were microinjected with the mixed AAV-Syn-Cre and AAV-Flex-sh*Best1*-GFP (or AAV-Flex-GFP) 14 days before PT surgery, and whole-cell currents were recorded on the pyramidal neurons of peri-infarct cortex during 12−24 h after PT (or sham) surgery. $n = 12$−14 neurons (from 6 to 7 mice). Data are mean ± SEM; $^*P < 0.05$, $^{**}P < 0.01$, $^{***}P < 0.001$.

a dramatic reduction of the tonic excitation when applied to slices from PT mice (Fig. 5I and J, $F_{(3,47)} = 34.16$, $P < 0.001$), suggesting BEST1 could be implicated in extrasynaptic glutamate release after ischemia. We further observed the influence of neuron-specific knockdown of BEST1 and found that the combination of AAV-Syn-Cre and AAV-Flex-shBEST1-GFP abolished NPPB-induced reduction of glutamate tonic excitation (Fig. 5I and J, $F_{(3,47)} = 34.16$, $P < 0.001$), indicating the inhibition of tonic glutamate excitation by NPPB was dependent on neuronal BEST1. Taken together, the results suggest that 12−24 h after PT, highly expressed BEST1 in neurons is responsible for the excessive extrasynaptic glutamate release, which could impel acute ischemic damage to become exacerbated.

3.6. Glutamate is released through neuronal BEST1 channel directly

Next, we tested whether glutamate could be released directly through neuronal BEST1 channel under ischemic condition. First, we carried out ion substitution experiments. We replaced Cl^- (146 mmol/L CsCl) in the internal pipette solution with equimolar glutamate (146 mmol/L CsGlutamate) and observed current-voltage relationships in $BEST1^{WT}$-expressing HEK293 cells. The findings demonstrated that heterogeneously expressed BEST1 showed an intracellular Ca^{2+}-dependent conductance of glutamate with reversal potential around −23.9 ± 3.2 mV, more negative than the reversal potential of Cl^- (−1.0 ± 1.1 mV) (Fig. 6A and B). Moreover, the permeability to glutamate almost disappeared when NPPB was applied to the external solution ($F_{(4,45)} = 14.96$, $P < 0.001$) or W93C mutation occurred in BEST1 ($F_{(4,45)} = 14.96$, $P < 0.001$) (Fig. 6A and B), implying channel function is required for glutamate permeability of BEST1. Then, we overexpressed $BEST1^{WT}$ in mice cortex with AAV-CMV-$BEST1^{WT}$-3Flag-T2A-GFP to determine the influence on OGD-induced anoxic depolarization (AD) current in slices. The effective infection of cortex neurons and the overexpression of BEST1 were verified 21 days after the virus microinjection (Fig. 6C and D). Consistent with previous report[25], OGD induced an obvious inward current in control slices (infected with AAV-CMV-3Flag-T2A-GFP), corresponding to AD (Fig. 6E). The OGD-induced current in $BEST1^{WT}$-overexpressed slices was larger (Fig. 6E and F, $F_{(2,32)} = 9.308$, $P = 0.009$), but almost abolished by concomitant application of AP-5 and CNQX with OGD (Fig. 6E and F, $F_{(2,32)} = 9.308$, $P = 0.001$), indicating glutamate release through overexpressed BEST1. When NPPB was contained in bath solution, OGD-induced AD current was slower in onset than normal (Fig. 6E and G) and more importantly BEST1-mediated AD current enlargement was absent (Fig. 6G and H, $t_{20} = 0.355$, $P = 0.726$). Therefore, we conclude that glutamate could be directly released through the BEST1 channel and

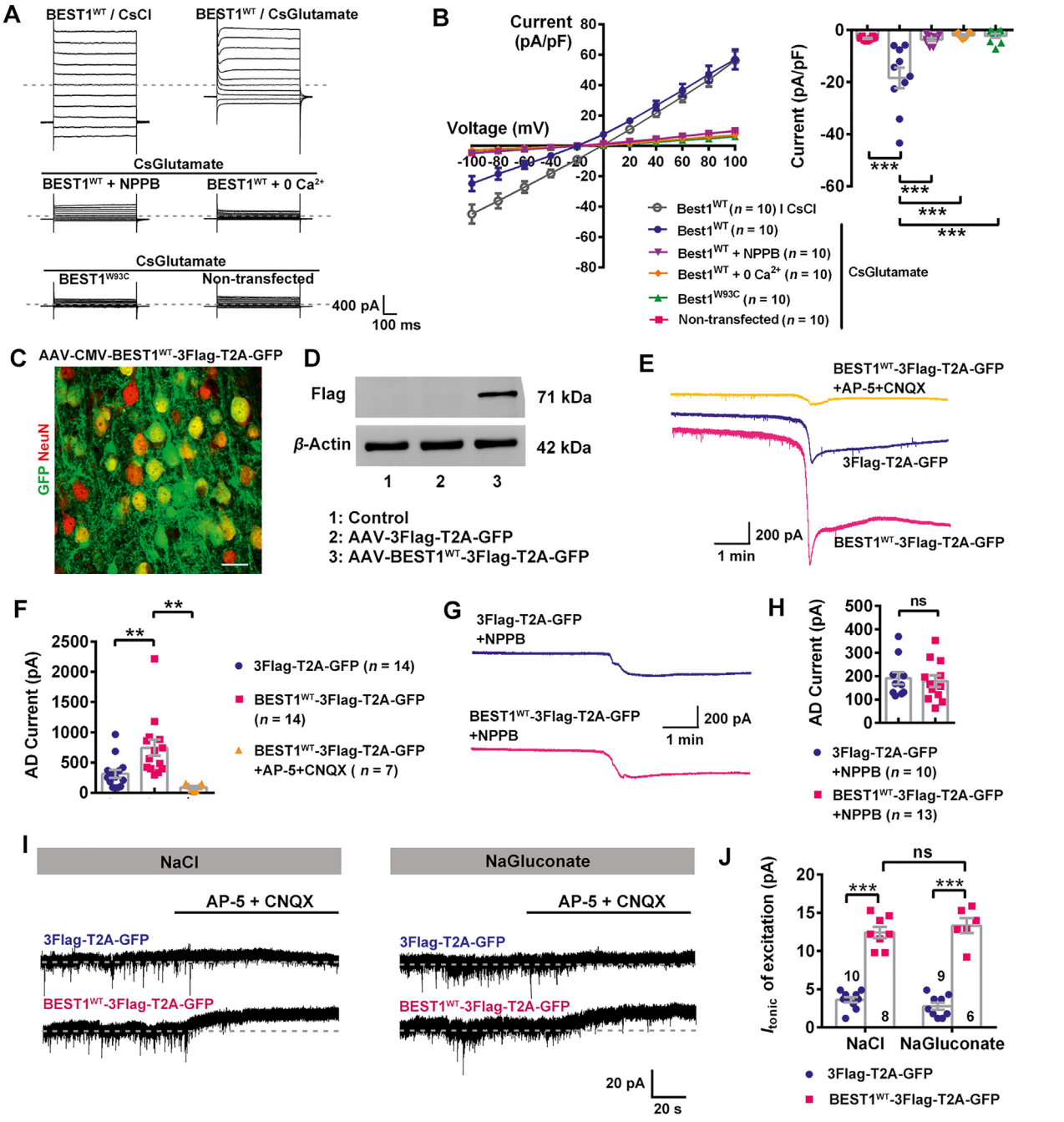

Figure 6 The role of chloride flux in BEST1-mediated glutamate release. (A) Representative current traces were recorded with whole-cell patch-clamp in HEK293 cells expressing mouse BEST1^{WT} or BEST1^{W93C}. To show glutamate permeability, the internal solution contained 146 mmol/L CsGlutamate instead of 146 mmol/L CsCl. Internal solution for all groups contained ~4.5 μmol/L Ca^{2+}, except 0 Ca^{2+} group. For NPPB group, 100 μmol/L NPPB was contained in external solution. (B) Current-voltage curves (left) and current amplitudes at −80 mV (right) quantified for the recordings are shown in (A). n = 10 cells (from 3 independent experiments). (C, D) Representative immunofluorescence image (C) and Western blots (D) showing effective BEST1^{WT}-3Flag expression in the cortex neurons of mice infected with AAV-CMV-BEST1^{WT}-3Flag-T2A-GFP 21 days after microinjection. Similar results were observed with 3 mice in each group. (E−H) Representative traces (E, G) and the scatter plot (F, H) showing OGD-induced AD current were recorded on cortex pyramidal neurons 21 days after the infection of AAV-CMV-BEST1^{WT}-3Flag-T2A-GFP or AAV-CMV-3Flag-T2A-GFP. n = 7 or 14 neurons (from 5 to 6 mice) for (F) and n = 10 or 13 neurons (from 5 to 6 mice) for (H). The concentration of AP-5, CNQX and NPPB was 50, 10 and 100 μmol/L, respectively. (I, J) Representative traces of sEPSCs with baseline shift (I) and scatter plot (J) showing the glutamate tonic excitation after AP-5 (50 μmol/L) and CNQX (10 μmol/L) application recorded on the pyramidal neurons of peri-infarct cortex 21 days after the infection of AAV-CMV-BEST1^{WT}-3Flag-T2A-GFP or AAV-CMV-3Flag-T2A-GFP. NaCl (125 mmol/L) in normal solution was replaced with NaGluconate (125 mmol/L) to obtain a low external Cl^- concentration. n = 6−10 neurons (from 3 to 5 mice). Data are mean ± SEM; $^{**}P < 0.01$, $^{***}P < 0.001$, ns = not significant. Scale bar, 20 μm.

BEST1-mediated glutamate release is dependent on the channel function of BEST1. These results from electrophysiological recordings supported the behavioral tests that overexpression of $BEST1^{W93C}$ attenuated acute ischemic damage. Finally, we recorded tonic glutamate excitation in a low external Cl^- solution in which 125 mmol/L NaCl was replaced with 125 mmol/L NaGluconate. Interestingly, the results showed that $BEST1^{WT}$ overexpression augmented tonic glutamate excitation in both external solutions (Fig. 6I and J, $F_{(1,29)} = 2.026$, $P < 0.001$) and there was no significance between I_{tonic} of $BEST1^{WT}$-overexpressed slices in NaCl solution and in NaGluconate solution (Fig. 6I and J, $F_{(1,29)} = 2.026$, $P = 0.920$), suggesting Cl^- flux is not necessary to BEST1-mediated glutamate release, though channel function of BEST1 is necessary. Taken together, glutamate could be released directly through the BEST1 channel to cause neuronal damage.

3.7. *Blocking BEST1 has a wide time window for treatment of ischemic damage*

Since reduced impairments of animal motor function were observed in mice with *Best1* shRNA knockdown or $BEST1^{W93C}$ mutation after ischemic damage, we further studied the time window for treatment. Considering the increased level of BEST1 expression during 8−48 h after PT, we supposed that blocking BEST1 would show neuroprotection in a relatively wide time window. Unfortunately, there is no specific blocker for BEST1, and various Cl^- channel blockers including NPPB were used in the study on BEST1. It was reported that 4,4′-diisothio-cyanostilbene-2,2′-disulfonic acid (DIDS) showed the highest selectivity for BEST1 among 7 inhibitors studied[50], and tonic release of glutamate by a DIDS-sensitive mechanism was discovered in rat hippocampal slices[51], so we employed DIDS to explore the time window for BEST1 inhibition. Based on the extracellular glutamate levels at 6 and 48 h after PT stroke (Fig. S5), DIDS was administrated for 4 consecutive days starting 6 h after ischemia at 12 mg/kg (Fig. 7A). The dose of DIDS was effective to suppress the BEST1 channel function (Supporting Information Fig. S9A and S9B). As expected, with this delayed treatment DIDS displayed the capability to suppress the expansion of infarct from 6 h to 73 h after PT ischemia (Fig. 7B and D, $F_{(2,35)} = 40.83$, $P = 0.001$) though the infarct volume at 73 h only showed a tendency to be smaller (Fig. B and C, $F_{(2,35)} = 32.09$, $P = 0.192$). The motor function impairments were alleviated in the cylinder task (Fig. 7E, $F_{(2,35)} = 64.33$, $P < 0.001$) and in the grid-walking task (Fig. 7F and G, $F_{(2,35)} = 64.48$, $P < 0.001$) for DIDS-treated mice. The improved motor function by DIDS treatment from 6 h could be observed until 28 days after PT (Supporting Information Fig. S10A−S10D, $F_{(6,168)} = 38.40$, $P < 0.001$ for Fig. S10B and $F_{(6,168)} = 58.55$, $P < 0.001$ for Fig. S10C), but DIDS treatment could not improve the motor functional impairment at both 78 h and 28 days when the administration began 12 h after PT (Fig. S10A−S10D). The body weight of DIDS-treated mice was similar with PT mice during the experiment (Fig. S10E). Moreover, the beneficial effects of DIDS delayed treatment were absent in mice with *Best1* shRNA knockdown (Supporting Information Fig. S11A−S11D), implying the necessary role of BEST1. Finally, we confirmed the influences of DIDS delayed treatment on infarct volume and neurological deficits with rat MCAO models (Fig. 7H). Consistent with the results from mouse PT models, smaller infarct volume (Fig. 7I and J, $F_{(2,39)} = 126.5$, $P = 0.003$) and lower neurological deficit scores (Fig. 7K, $F_{(2,39)} = 7.291$, $P = 0.040$) were observed in DIDS-treated PT rats than vehicle-treated ones 2 days after MCAO. Therefore, our findings suggest that blocking BEST1 with DIDS is beneficial to suppress the infract expansion and attenuate the function impairments even 6 h after ischemia.

4. Discussion

In this paper, we reported the important contribution of neuronal glutamate-releasing BEST1 channel in the peri-infarct zone to the exacerbation of ischemic damage from 8 to 48 h after ischemic stroke in rodents. BEST1-mediated glutamate release was extrasynaptic, leading to the enhancement of tonic excitation and delayed excitotoxicity. Interfering the protein expression or inhibiting the channel function of BEST1 by genetic manipulation or pharmacological antagonism improved motor functional deficits. Therefore, this study suggests that glutamate-releasing BEST1 channel is a potential target for neuroprotection against ischemic damage with wide time window.

Excessive glutamate release after ischemia results in acute neuronal damage and death, which is named excitotoxicity. Though the mechanism of glutamate release is controversial, evidence supports that exocytosis through synaptic vesicle does not contribute much because the glutamate release induced by ischemia was Ca^{2+}-independent and could not been prevented by bafilomycin A1, a vacuolar-type H^+-ATPase inhibitor[16−18,25]. The extrasynaptic release pattern is probably due to low ATP and GTP levels after ischemia[52]. Reversed glutamate transporters played the most important role in the extrasynaptic release of glutamate within a few minutes after the start of ischemia *in vitro*[18]; however, EAATs expression in focal transient ischemic rat cortex decreased from Day 1 to Day 7 after perfusion[53], indicating less contribution to persistent glutamate release. Extrasynaptic glutamate release through ion channels and other ways are also suggested to be involved in ischemic acute injury, such as acid-sensitive ion channel ASIC1a in transient rat global ischemia[54], volume-regulated anion channel SWELL1 in mice MCAO model[26], neuronal gap junction hemichannel pannexin 1 in OGD-exposed neurons *in vitro*[55] and cystine/glutamate antiporter in OGD-exposed slices *in vitro*[25]. They were almost stimulated within several minutes to hours after ischemia. In this study, we demonstrated a delayed glutamate release mechanism through a calcium-activated chloride channel BEST1 which was prominent from 8 to 48 h after mice PT ischemia and also contributed to injury deterioration and infarct expansion in rat MCAO ischemia. Therefore, the mechanism by which glutamate is released is likely multi-factorial and depends on the severity of the ischemic stroke, the ischemic model used and the stage of ischemic injury[16,18]. No doubt that the immediate molecular events within the first few hours after stroke are crucial to the acute ischemic injury and determine the final infarct and functional outcome in large part. Unfortunately, the irreversible neuronal death in the ischemic core and the narrow time window for treatment limit the effective clinical translation of the logical neuroprotective approaches targeting such immediate molecules. Given that ischemic stroke involves a core expansion over days[56], treatment with an extended time window is anticipated. At least, BEST1-mediated delayed glutamate release contributes to the progress from initial injury to final infarct. Besides excessive glutamate release, reduced GLT-1 expression[53] or activity[57] after MCAO was also suggested to lead to impaired glutamate uptake quickly. In this study, we did not find a downregulation of expression or function of GLT-1,

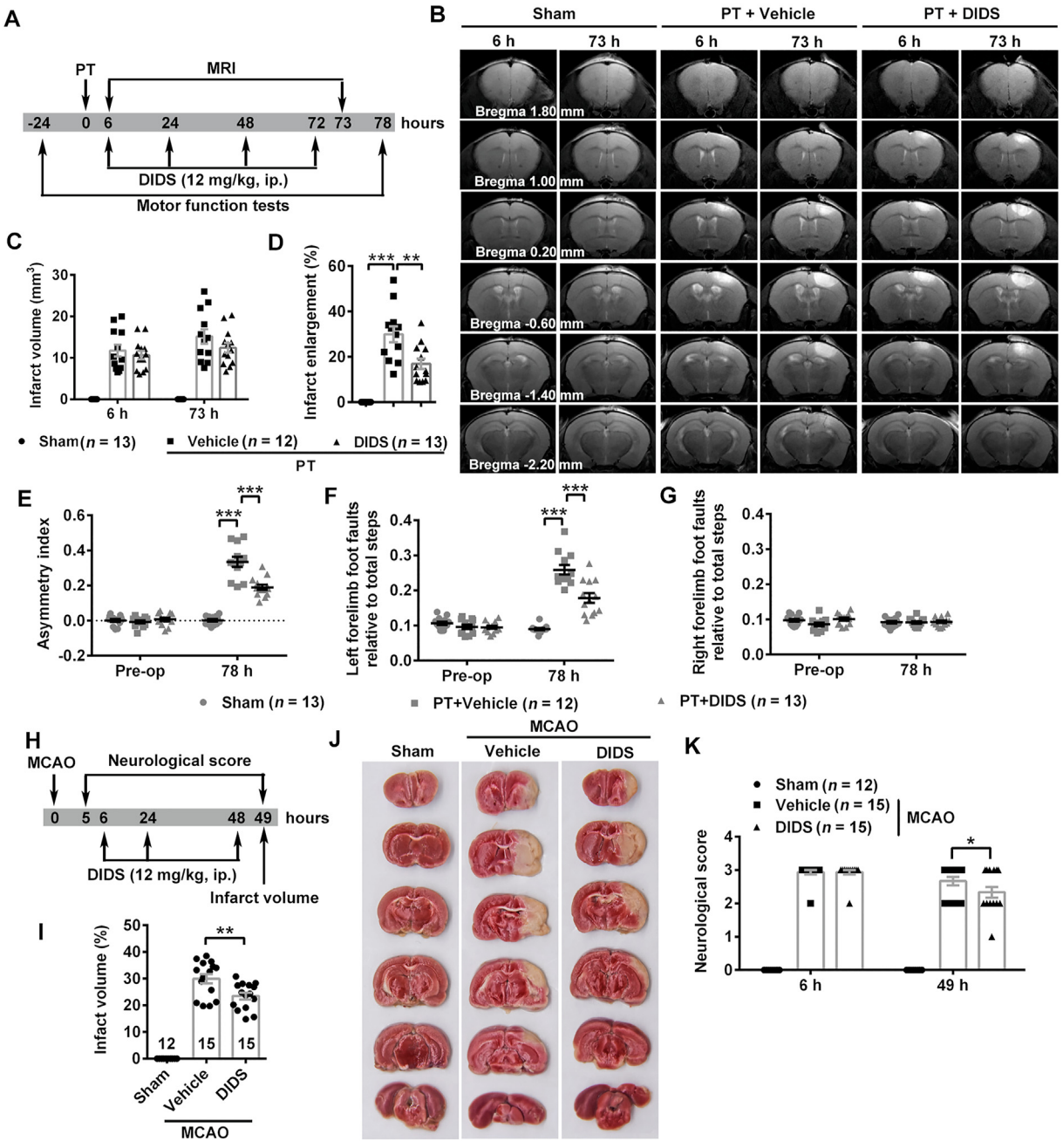

Figure 7 The effects of DIDS delayed treatment on animal ischemic models. (A) The scheme of experimental design for mouse PT models. (B−D) Representative T2-weighted MRI scanning images (B) and scatter plots showing the infarct volume at 6 h and 73 h after mouse PT ischemia (C, $n = 12-13$) and the infarct enlargement from 6 h to 73 h (D, $n = 12-13$). (E−G) Scatter plots showing forelimb asymmetry (E) in cylinder task, foot faults of left (F) and right (G) forelimb in grid-walking task. $n = 12-13$. One mouse in PT + Vehicle group escaped. (H) The scheme of experimental design for rat MCAO models. (I, J) Scatter plot (I) and TTC staining images (J) showing the infarct volume at 49 h after rat MCAO. (K) Scatter plot showing the scores of neurological deficits. $n = 12$ or 15. Data are mean ± SEM; $^{*}P < 0.05$, $^{**}P < 0.01$, $^{***}P < 0.001$.

probably due to mild injury after PT stroke. However, we observed a decreased tendency of GLT-1 expression at 8 h after PT. The contribution of impaired glutamate uptake through GLT-1 to acute ischemic injury could not be excluded during severe ischemia.

It is well known that many NMDAR antagonists have failed in clinical trials. Besides the serious side effects, another important problem is the limited time window for effective drug administration, which makes NMDAR antagonists therapeutically impractical. By specifically targeting downstream signaling proteins of GluN2B-mediating pro-death pathway, it may be possible to develop therapeutics with fewer side effects and wider treatment window[9]. Fortunately, in a multicentre, double-blind, randomized controlled trial (ESCAPE-NA1 phase 3 trial), nerinetide,

an eicosapeptide which was designed to perturb the protein−protein interaction of GluN2B and PSD-95, was observed to reduce median infarct volumes and improved outcomes in the no alteplase stratum[11]. In this study, patients with acute ischemic stroke due to large vessel occlusion within a 12 h treatment window were enrolled, breaking the time window limitation of neuroprotectants. In our study, we found a delayed BEST1-mediated glutamate release after stroke leading to the exacerbation of ischemic damage in rodents, which gave a 6 h time window for effective treatment of BEST1 blockers, further confirming the proper neuroprotection against excitotoxicity would be effective in a wide time window.

Most of the researches on the function of BEST1 in the brain came from the lab of Dr. Lee. They established the relationship of GABA- or glutamate-releasing and Cl^- permeability of BEST1 in astrocytes under physiological conditions[32−34]; however, the Cl^- permeability of astrocytic BEST1 was not mentioned in their later papers on Alzheimer's disease[36], motor coordination[35] and subcortical ischemic stroke[38]. Consistently, we found that neuronal BEST1-mediated glutamate releasing was accompanied with increased Cl^- permeability of the channel after cerebral ischemia and could be inhibited by $BEST1^{W93C}$ mutation impairing the Cl^- currents. There was a possibility that glutamate-releasing was dependent on the permeation of Cl^- through BEST1. Interestingly, our results from Cl^- substitution experiment demonstrated that Cl^- flux was not required for glutamate releasing. The high Cl^- permeability did not bring the real Cl^- flux through BEST1, which is probably due to increased intracellular concentration of Cl^- during ischemia[58,59]. For neurons in the brain, Cl^- ion homeostasis is maintained principally by Na^+−K^+−Cl^- co-transporter 1 (NKCC1) and K^+−Cl^- co-transporter 2 (KCC2), the former pumping in extracellular Cl^- at the ratio of 1 Na^+:1 K^+:2 Cl^- and the latter pumping out intracellular Cl^- at the ratio of 1 K^+:1 Cl^-[60,61]. Under physiological conditions in adults, highly expressed KCC2 compared to NKCC1 maintains a low intracellular Cl^- concentration, and NKCC1 upregulation and/or KCC2 downregulation are supposed to participate in many neurological disorders, including cerebral stroke[59,62]. Thus, the role of BEST1 as a Cl^- channel in cerebral neurons is not as important as in the retina. At least, our results indicate that BEST1 is more like a glutamate channel than a Cl^- channel in the peri-infarct cortex. On the other hand, the high Cl^- permeability of neuronal BEST1 channel facilitates the glutamate-releasing after ischemia, like glutamate-releasing from astrocytic SWELL1 channel[26].

Besides BEST1, other Cl^- channels such as TMEM16 and LRRC8A (also known as SWELL1) are implicated in diverse nerve functions including nociception, olfactory transduction, neuronal excitability, action potential and synaptic response[26,63−65]. Unfortunately, there is no specific inhibitor for these Cl^- channels. NPPB and DIDS are commonly used in the studies of BEST1 channels[32−34,36]. By systematic comparison with patch clamp technique, DIDS displayed the highest selectivity for BEST1 over TMEM16A in seven Cl^- channel inhibitors studied[50]. Thus, we chose DIDS to test the time window of neuroprotection of BEST1 inhibition in animal experiments. This broad-spectrum Cl^- channels and transporters blocker has shown remarkable promise as a cytoprotective agent against ischemic insults in cultured neurons or slices in early studies[66−69]. Furthermore, in an *in vivo* transient forebrain ischemia model, DIDS could attenuate delayed neuronal death in hippocampal CA1 neurons[70]. Regretfully, no more significant study was reported about the further application of DIDS against cerebral ischemia. Obviously, the broad antagonism to Cl^- channels and transporters is an outstanding question for DIDS, moreover, the action of DIDS is not cell-specific. Though the efficacy of DIDS to attenuate infarct expansion and ameliorate neurological deficits in rodents have been demonstrated in this study, specific and potent blocker of BEST1 would be more valuable in ischemic stroke treatment. Structure modification of DIDS or completely novel compound targeting BEST1 must be developed to fully exploit the therapeutic potential of BEST1 inhibition and more work is needed to translate these promising results into effective stroke therapies.

Finally, we have to point out that the knockdown of BEST1 in the brain was performed only using sh*Best1*-containing AAVs. Though we have validated the effectiveness and specificity of BEST1 knockdown within the peri-infarct cortex, the effect was local and weak owing to the dependence of AAV infection and expression. This might give rise to an underestimation of the influence of BEST1 downregulation, including the possible toxicity. Neuron-specific and astrocyte-specific BEST1 conditional knockout mice would be employed in future study to further evaluate BEST1 as a drug target.

5. Conclusions

Our study demonstrates that neuronal BEST1-mediated extrasynaptic glutamate release results in delayed excitotoxicity and BEST1 channels can serve as a potential therapeutic target against ischemic stroke with a wide time window.

Acknowledgments

This study was supported by STI2030-Major Project (2022ZD0211700, China), National Natural Science Foundation of China (82171293, 82090042 and 82171368), Natural Science Foundation of Jiangsu Province (BK20211255, China). The authors would like to thank Aixia Zhang for helpful advice about cell cultures, and Tengfei Ma for electrophysiological recordings.

Author contributions

Shuai Xiong, Hui Xiao, Meng Sun and Yunjie Liu carried out and analyzed behavioral tests. Hui Xiao, Ke Xu, and Haiying Liang performed fluorescent imaging experiments and biochemical assays. Shuai Xiong, Ling Gao and Yuihui Lin performed and analyzed electrophysiological recordings. Lei Chang and Haiyin Wu prepared animal models and conducted microinjections. Shuai Xiong and Hui Xiao cultured cells. Chunxia Luo, Dongya Zhu and Nan Jiang designed research. Chunxia Luo and Dongya Zhu directed experiments. Chunxia Luo wrote the paper. All authors have read and approved the final manuscript.

Conflicts of interest

The authors declare no conflicts of interest.

Appendix A. Supporting information

Supporting data to this article can be found online at https://doi.org/10.1016/j.apsb.2023.05.012.

References

1. Powers WJ, Rabinstein AA, Ackerson T, Adeoye OM, Bambakidis NC, Becker K, et al. 2018 Guidelines for the early management of patients with acute ischemic stroke: a guideline for healthcare professionals from the American heart association/American stroke association. *Stroke* 2018;**49**:e46−110.
2. Powers WJ, Rabinstein AA, Ackerson T, Adeoye OM, Bambakidis NC, Becker K, et al. Guidelines for the early management of patients with acute ischemic stroke: 2019 update to the 2018 guidelines for the early management of acute ischemic stroke: a guideline for healthcare professionals from the American heart association/American stroke association. *Stroke* 2019;**50**:e344−418.
3. Moskowitz MA, Lo EH, Iadecola C. The science of stroke: mechanisms in search of treatments. *Neuron* 2010;**67**:181−98.
4. Yang Q, Huang Q, Hu Z, Tang X. Potential neuroprotective treatment of stroke: targeting excitotoxicity, oxidative stress, and inflammation. *Front Neurosci* 2019;**13**:1036.
5. Chen X, Zhang J, Wang K. Inhibition of intracellular proton-sensitive Ca^{2+}-permeable TRPV3 channels protects against ischemic brain injury. *Acta Pharm Sin B* 2022;**12**:2330−47.
6. Kikuchi K, Tanaka E, Murai Y, Tancharoen S. Clinical trials in acute ischemic stroke. *CNS Drugs* 2014;**28**:929−38.
7. Reis C, Akyol O, Ho WM, Araujo C, Huang L, Applegate II R, et al. Phase I and phase II therapies for acute ischemic stroke: an update on currently studied drugs in clinical research. *BioMed Res Int* 2017;**2017**:4863079.
8. Xue T, Ji J, Sun Y, Huang X, Cai Z, Yang J, et al. Sphingosine-1-phosphate, a novel TREM2 ligand, promotes microglial phagocytosis to protect against ischemic brain injury. *Acta Pharm Sin B* 2022;**12**:1885−98.
9. Lai TW, Zhang S, Wang YT. Excitotoxicity and stroke: identifying novel targets for neuroprotection. *Prog Neurobiol* 2014;**115**:157−88.
10. Zhou L, Li F, Xu HB, Luo CX, Wu HY, Zhu MM, et al. Treatment of cerebral ischemia by disrupting ischemia-induced interaction of nNOS with PSD-95. *Nat Med* 2010;**16**:1439−43.
11. Hill MD, Goyal M, Menon BK, Nogueira RG, McTaggart RA, Demchuk AM, et al. Efficacy and safety of nerinetide for the treatment of acute ischaemic stroke (ESCAPE-NA1): a multicentre, double-blind, randomised controlled trial. *Lancet* 2020;**395**:878−87.
12. Zhou XF. ESCAPE-NA1 trial brings hope of neuroprotective drugs for acute ischemic stroke: highlights of the phase 3 clinical trial on nerinetide. *Neurosci Bull* 2021;**37**:579−81.
13. Muir KW, Lees KR, Ford I, Davis S. Intravenous magnesium efficacy in stroke (IMAGES) study investigators. Magnesium for acute stroke (intravenous magnesium efficacy in stroke trial): randomised controlled trial. *Lancet* 2004;**363**:439−45.
14. Valentino K, Newcomb R, Gadbois T, Singh T, Bowersox S, Bitner S, et al. A selective N-type calcium channel antagonist protects against neuronal loss after global cerebral ischemia. *Proc Natl Acad Sci U S A* 1993;**90**:7894−7.
15. Muir KW, Holzapfel L, Lees KR. Phase II clinical trial of sipatrigine (619C89) by continuous infusion in acute stroke. *Cerebrovasc Dis* 2000;**10**:431−6.
16. Drejer J, Benveniste H, Diemer NH, Schousboe A. Cellular origin of ischemia-induced glutamate release from brain tissue *in vivo* and *in vitro*. *J Neurochem* 1985;**45**:145−51.
17. Phillis JW, Ren J, O'Regan MH. Transporter reversal as a mechanism of glutamate release from the ischemic rat cerebral cortex: studies with DL-threo-beta-benzyloxyaspartate. *Brain Res* 2000;**868**:105−12.
18. Rossi DJ, Oshima T, Attwell D. Glutamate release in severe brain ischaemia is mainly by reversed uptake. *Nature* 2000;**403**:316−21.
19. Colleoni S, Jensen AA, Landucci E, Fumagalli E, Conti P, Pinto A, et al. Neuroprotective effects of the novel glutamate transporter inhibitor (−)-3-hydroxy-4,5,6,6a-tetrahydro-3a*H*-pyrrolo[3,4-*d*]-isoxazole-4-carboxylic acid, which preferentially inhibits reverse transport (glutamate release) compared with glutamate reuptake. *J Pharmacol Exp Therapeut* 2008;**326**:646−56.
20. Rothstein JD, Dykes-Hoberg M, Pardo CA, Bristol LA, Jin L, Kuncl RW, et al. Knockout of glutamate transporters reveals a major role for astroglial transport in excitotoxicity and clearance of glutamate. *Neuron* 1996;**16**:675−86.
21. Rothstein JD, Jin L, Dykes-Hoberg M, Kuncl RW. Chronic inhibition of glutamate uptake produces a model of slow neurotoxicity. *Proc Natl Acad Sci U S A* 1993;**90**:6591−5.
22. Rao VL, Dogan A, Todd KG, Bowen KK, Kim BT, Rothstein JD, et al. Antisense knockdown of the glial glutamate transporter GLT-1, but not the neuronal glutamate transporter EAAC1, exacerbates transient focal cerebral ischemia-induced neuronal damage in rat brain. *J Neurosci* 2001;**21**:1876−83.
23. Rothstein JD, Patel S, Regan MR, Haenggeli C, Huang YH, Bergles DE, et al. Beta-lactam antibiotics offer neuroprotection by increasing glutamate transporter expression. *Nature* 2005;**433**:73−7.
24. Thöne-Reineke C, Neumann C, Namsolleck P, Schmerbach K, Krikov M, Schefe JH, et al. The beta-lactam antibiotic, ceftriaxone, dramatically improves survival, increases glutamate uptake and induces neurotrophins in stroke. *J Hypertens* 2008;**26**:2426−35.
25. Soria FN, Pérez-Samartín A, Martin A, Gona KB, Llop J, Szczupak B, et al. Extrasynaptic glutamate release through cystine/glutamate antiporter contributes to ischemic damage. *J Clin Invest* 2014;**124**:3645−55.
26. Yang J, Vitery MDC, Chen J, Osei-Owusu J, Chu J, Qiu Z. Glutamate-releasing SWELL1 channel in astrocytes modulates synaptic transmission and promotes brain damage in stroke. *Neuron* 2019;**102**:813−27.
27. Lin YH, Dong J, Tang Y, Ni HY, Zhang Y, Su P, et al. Opening a new time window for treatment of stroke by targeting HDAC2. *J Neurosci* 2017;**37**:6712−28.
28. Hartzell HC, Qu Z, Yu K, Xiao Q, Chien LT. Molecular physiology of bestrophins: multifunctional membrane proteins linked to best disease and other retinopathies. *Physiol Rev* 2008;**88**:639−72.
29. Kane Dickson V, Pedi L, Long SB. Long, structure and insights into the function of a Ca^{2+}-activated Cl^{-} channel. *Nature* 2014;**516**:213−8.
30. Oh SJ, Lee CJ. Distribution and function of the Bestrophin-1 (Best1) channel in the brain. *Exp Neurobiol* 2017;**26**:113−21.
31. Petrukhin K, Koisti MJ, Bakall B, Li W, Xie G, Marknell T, et al. Identification of the gene responsible for Best macular dystrophy. *Nat Genet* 1998;**19**:241−7.
32. Park H, Oh SJ, Han KS, Woo DH, Park H, Mannaioni G, et al. Bestrophin-1 encodes for the Ca^{2+}-activated anion channel in hippocampal astrocytes. *J Neurosci* 2009;**29**:13063−73.
33. Lee S, Yoon BE, Berglund K, Oh SJ, Park H, Shin HS, et al. Channel-mediated tonic GABA release from glia. *Science* 2010;**330**:790−6.
34. Woo DH, Han KS, Shim JW, Yoon BE, Kim E, Bae JY, et al. TREK-1 and Best1 channels mediate fast and slow glutamate release in astrocytes upon GPCR activation. *Cell* 2012;**151**:25−40.
35. Woo J, Min JO, Kang DS, Kim YS, Jung GH, Park HJ, et al. Control of motor coordination by astrocytic tonic GABA release through modulation of excitation/inhibition balance in cerebellum. *Proc Natl Acad Sci U S A* 2018;**115**:5004−9.
36. Jo S, Yarishkin O, Hwang YJ, Chun YE, Park M, Woo DH, et al. GABA from reactive astrocytes impairs memory in mouse models of Alzheimer's disease. *Nat Med* 2014;**20**:886−96.
37. Pandit S, Neupane C, Woo J, Sharma R, Nam MH, Lee GS, et al. Bestrophin1-mediated tonic GABA release from reactive astrocytes prevents the development of seizure-prone network in kainate-injected hippocampi. *Glia* 2020;**68**:1065−80.
38. Nam MH, Cho J, Kwon DH, Park JY, Woo J, et al. Excessive astrocytic GABA causes cortical hypometabolism and impedes functional recovery after subcortical stroke. *Cell Rep* 2020;**32**:107861.
39. Boudes M, Sar C, Menigoz A, Hilaire C, Péquignot MO, Kozlenkov A, et al. Best1 is a gene regulated by nerve injury and

required for Ca^{2+}-activated Cl^- current expression in axotomized sensory neurons. *J Neurosci* 2009;**29**:10063−71.
40. Boudes M, Scamps F. Calcium-activated chloride current expression in axotomized sensory neurons: what for? *Front Mol Neurosci* 2012; **5**:5.
41. Lin YH, Liang HY, Xu K, Ni HY, Dong J, Xiao H, et al. Dissociation of nNOS from PSD-95 promotes functional recovery after cerebral ischaemia in mice through reducing excessive tonic GABA release from reactive astrocytes. *J Pathol* 2018;**244**:176−88.
42. Qu Z, Chien LT, Cui Y, Hartzell HC. The anion-selective pore of the bestrophins, a family of chloride channels associated with retinal degeneration. *J Neurosci* 2006;**26**:5411−9.
43. Liang HY, Chen ZJ, Xiao H, Lin YH, Hu YY, Chang L, et al. nNOS-expressing neurons in the vmPFC transform pPVT-derived chronic pain signals into anxiety behaviors. *Nat Commun* 2020;**11**:2501.
44. Lin Y, Yao M, Wu H, Wu F, Cao S, Ni H, et al. Environmental enrichment implies GAT-1 as a potential therapeutic target for stroke recovery. *Theranostics* 2021;**11**:3760−80.
45. Luo CX, Lin YH, Qian XD, Tang Y, Zhou HH, Jin X, et al. Interaction of nNOS with PSD-95 negatively controls regenerative repair after stroke. *J Neurosci* 2014;**34**:13535−48.
46. Li J, Zhang L, Xu C, Shen YY, Lin YH, Zhang Y, et al. A pain killer without analgesic tolerance designed by co-targeting PSD-95-nNOS interaction and α2-containning $GABA_A$Rs. *Theranostics* 2021;**11**: 5970−85.
47. Ortinski PI, Turner JR, Pierce RC. Extrasynaptic targeting of NMDA receptors following D1 dopamine receptor activation and cocaine self-administration. *J Neurosci* 2013;**33**:9451−61.
48. Neupane C, Sharma R, Pai YH, Lee SY, Jeon BH, Kim HW, et al. High salt intake recruits tonic activation of NR2D subunit-containing extrasynaptic NMDARs in vasopressin neurons. *J Neurosci* 2021;**41**: 1145−56.
49. Wang XN, Liu JQ, Shi ZQ, Sun FY, Liu LF, Xin GZ. Orthogonal label and label-free dual pretreatment for targeted profiling of neurotransmitters in enteric nervous system. *Anal Chim Acta* 2020;**1139**: 68−78.
50. Liu Y, Zhang H, Huang D, Qi J, Xu J, Gao H, et al. Characterization of the effects of Cl^- channel modulators on TMEM16A and bestrophin-1 Ca^{2+} activated Cl^- channels. *Pflügers Archiv* 2015;**467**:1417−30.
51. Cavelier P, Attwell D. Tonic release of glutamate by a DIDS-sensitive mechanism in rat hippocampal slices. *J Physiol* 2005;**564**:397−410.
52. Szatkowski M, Attwell D. Triggering and execution of neuronal death in brain ischaemia: two phases of glutamate release by different mechanisms. *Trends Neurosci* 1994;**17**:359−65.
53. Sánchez-Mendoza E, Burguete MC, Castelló-Ruiz M, González MP, Roncero C, Salom JB, et al. Transient focal cerebral ischemia significantly alters not only EAATs but also VGLUTs expression in rats: relevance of changes in reactive astroglia. *J Neurochem* 2010; **113**:1343−55.
54. Gao J, Duan B, Wang DG, Deng XH, Zhang GY, Xu L, et al. Coupling between NMDA receptor and acid-sensing ion channel contributes to ischemic neuronal death. *Neuron* 2005;**48**:635−46.
55. Thompson RJ, Zhou N, MacVicar BA. Ischemia opens neuronal gap junction hemichannels. *Science* 2006;**312**:924−7.
56. Lo EH. A new penumbra: transitioning from injury into repair after stroke. *Nat Med* 2008;**14**:497−500.
57. Wang Y, Lu S, Chen Y, Li L, Li X, Qu Z, et al. Smoothened is a therapeutic target for reducing glutamate toxicity in ischemic stroke. *Sci Transl Med* 2021;**13**:eaba3444.
58. Pond BB, Berglund K, Kuner T, Feng G, Augustine GJ, Schwartz-Bloom RD. The chloride transporter Na^+−K^+−Cl^--cotransporter isoform-1 contributes to intracellular chloride increases after *in vitro* ischemia. *J Neurosci* 2006;**26**:1396−406.
59. Martín-Aragón Baudel MA, Poole AV, Darlison MG. Chloride co-transporters as possible therapeutic targets for stroke. *J Neurochem* 2017;**140**:195−209.
60. Blaesse P, Airaksinen MS, Rivera C, Kaila K. Cation−chloride cotransporters and neuronal function. *Neuron* 2009;**61**:820−38.
61. Kaila K, Price TJ, Payne JA, Puskarjov M, Voipio J. Cation−chloride cotransporters in neuronal development, plasticity and disease. *Nat Rev Neurosci* 2014;**15**:637−54.
62. Savardi A, Borgogno M, De Vivo M, Cancedda L. Pharmacological tools to target NKCC1 in brain disorders. *Trends Pharmacol Sci* 2021; **42**:1009−34.
63. Kunzelmann K. TMEM16, LRRC8A, bestrophin: chloride channels controlled by Ca^{2+} and cell volume. *Trends Biochem Sci* 2015;**40**: 535−43.
64. Cho H, Yang YD, Lee J, Lee B, Kim T, Jang Y, et al. The calcium-activated chloride channel anoctamin 1 acts as a heat sensor in nociceptive neurons. *Nat Neurosci* 2012;**15**:1015−21.
65. Huang WC, Xiao S, Huang F, Harfe BD, Jan YN, et al. Calcium-activated chloride channels (CaCCs) regulate action potential and synaptic response in hippocampal neurons. *Neuron* 2012;**74**:179−92.
66. Malek SA, Coderre E, Stys PK. Aberrant chloride transport contributes to anoxic/ischemic white matter injury. *J Neurosci* 2003;**23**: 3826−36.
67. Yao H, Sun X, Gu X, Wang J, Haddad GG. Cell death in an ischemic infarct rim model. *J Neurochem* 2007;**103**:1644−53.
68. Yao H, Felfly H, Wang J. DIDS protects against neuronal injury by blocking Toll-like receptor 2 activated-mechanisms. *J Neurochem* 2009;**108**:835−46.
69. Pamenter ME, Ryu J, Hua ST, Perkins GA, Mendiola VL, Gu XQ, et al. DIDS prevents ischemic membrane degradation in cultured hippocampal neurons by inhibiting matrix metalloproteinase release. *PLoS One* 2012;**7**:e43995.
70. Inoue H, Ohtaki H, Nakamachi T, Shioda S, Okada Y. Anion channel blockers attenuate delayed neuronal cell death induced by transient forebrain ischemia. *J Neurosci Res* 2007;**85**:1427−35.